Guardiola, C.; Pla Moreno, B.; Blanco-Rodriguez, D.; Calendini, PO. (2015). ECU-oriented models for NOx prediction. Part 1: a mean value engine model for NOx prediction. Proceedings of the Institution of Mechanical Engineers, Part D: Journal of Automobile Engineering. 229(8):992-1015. doi:10.1177/0954407014550191.

ECU oriented models for NO_x prediction. Part 1: A mean value engine model for NO_x prediction

C.Guardiola, B.Pla, D.Blanco-Rodriguez

CMT Motores Térmicos, Universitat Politècnica de Valéncia, Camino de Vera s/n, E-46022 Valencia, Spain

P.O. Calendini

Diesel Engine Control Department, PSA Peugeot Citroën, 18 rue des Fauvelles, 92256 La Garenne Colombes, France

Abstract

The implantation of NO_x sensors in diesel engines is necessary in order to track emissions at the engine exhaust for diagnosing and control of the after-treatment devices. However, the use of models is still necessary as the output from these sensors is delayed and filtered. The present paper deals with the problem of NO_x estimation in two parts covering modelling and data fusion of a sensor signal and the model, respectively. This is the first part where a NO_x model is developed based on a nominal set-point relative fitting of the NO_x with a series of corrections for accounting with variations on λ^{-1}, temperatures and other signals. The NO_x model combines look-up tables with physical-based equations and is designed for being implemented on commercial ECUs. The relatively low calibration effort and the reported results presented with a turbocharged diesel engine shows the feasibility of the model and the possibilities for on-board implementation. This paper is the first part of a two-parts paper dedicated to the on-board estimation of NO_x.

Keywords: NO_x model; look-up tables; diesel engine; NO_x sensor; control
PACS: 5.70.a, 89.40.Bb

1. Introduction

The world attention about environmental protection has resulted in new strict laws which establish the requirements for pollutant emissions, and therefore define priorities in the technology development [1]. In such sense, the Euro standards [2] fix the emissions limits for NO_x and PM for the European Union mobile sources. Concretely, light-duty diesel engines must reduce NO_x emissions by 20% with regards to EURO 5 and 50% with regards to EURO 6 if comparing with previous EURO 4 standard.

The monitoring of emissions in diesel engines require the use of sensors, model based strategies or a combination of both. For instance, the dynamic responses of the on-board sensors are limited, and then models are still necessary. This paper focuses on the development of an ECU-oriented NO_x model for predicting NO_x emissions at the engine exhaust. This model is based on

Email addresses: carguaga@mot.upv.es (C.Guardiola), benplamo@mot.upv.es (B.Pla), dablarod@mot.upv.es (D.Blanco-Rodriguez), pierreolivier.calendini@mpsa.com (P.O. Calendini)

maps that get the nominal behaviour of the engine according to the injected fuel mass flow and the engine speed, and different corrections for coping with the boost pressure and temperature, air mass flow, coolant temperature, humidity and in-cylinder temperature variations at conditions different to the base calibration. Provided that if the engine is running slowly among different engine operating points, the base maps can be enough for retrieving the model outputs, these corrections are needed when the engine runs in transients. In addition, the text gives hints on how to consider injection timing variations and indeed a multi-mode approach when the engine is running cold. All required inputs for the model, excepting the humidity, come from available signals in standard ECUs. The model is validated for a steady-state data set and in different engine dynamic cycles for a turbocharged diesel engine.

After-treatment systems are not considered but the model is still valid for predicting exhaust NO_x emissions, being able to use it in the diagnosis and control of SCR or LNT, when a NO_x sensor is installed downstream of them. Furthermore, if SCR or LNT are modelled, the model can be extended for predicting pipe-out NO_x. Finally, the model is valid without the presence of a N O $_x$ sensor for estimating raw engine exhaust emissions.

2. Review of the background for modelling NO_x in diesel engines

The term NO_x includes all nitrogen oxides, but it is the nitric oxide (NO) the predominant at the diesel engine exhaust [3]. The NO_x formation is affected by three different mechanisms: thermal, prompt and from fuel-bound nitrogen [4]. The thermal mechanism is the most relevant in diesel engines where high temperatures benefit reaction of N and O_2 from air producing NO_x. NO_x formation physics in combustion and explosion processes were modelled by Zeldovych [5] in 1946, and formulated for IC engines by Lavoie *et al.* [6] in 1970 with the well-known extended-Zeldovych mechanism

$$\begin{array}{rcl} N + NO & \rightleftarrows & NO_2 \\ N + O_2 & \rightleftarrows & NO + O \\ N + OH & \rightleftarrows & NO + H \end{array} \tag{1}$$

According to Heywood [3], the typical characteristic times of the NO formation in diesel engines combustion are in the order of seconds and thus under the hypothesis of equilibrium of certain species, the dNO/dt can be fitted with the initial NO formation rate by the Arrhenius equation

$$\frac{dNO}{dt} = \frac{k_1}{T^{0.5}} e^{-k_2/T} [O_2]^{0.5} [N] \tag{2}$$

The strong dependency with the temperature T is clear: when T increases, NO (and thus NO_x) increases exponentially. The other mechanisms can be relevant in some specific conditions such as LTC [7, 8].

The cylinder conditions, namely temperature, pressure and oxygen concentration [9, 10, 11], are the most important variables for determining NO_x concentration at the engine exhaust. But because of the cylinder severe conditions, price and signals problems have prevented to use in-cylinder sensors in commercial vehicles. Despite all of these, the continuous improvements of pressure sensors and their applications are justifying its nearby implementation [12]. The case of the temperature sensors is more complicated [13], and their use is not foreseen in applications. Therefore, the solution for estimating in-cylinder conditions on real-time is using virtual sensors.

Physical models for NO_x estimation are often based in the heat release, using the pressure sensor signal for estimating flame temperature (T_f) in the cylinder. The problem is not trivial and a multi-zone discretisation is advisable. Furthermore, the residual gasses (internal EGR) affect the process and these are not always easy to estimate. An usual solution to the problem is applying mass and energy conservation equations to each zone (walls, injector neighbourhood, etc.) in conjunction with heat transfer equations, among them it stands out the heat transfer to the cylinder walls [14], which could be approached by using Woschni equation [15]. Finally, NO_x emissions are calculated by using the extended Zeldovych mechanism. Good examples for estimating NO_x by using heat release are [16, 17, 18, 19]. In the case of SI engines, [20, 21] use ionisation current on spark for approaching pressure, but this is not available in diesel engines. The accuracy of the prediction anyhow is not as satisfactory as expected, and the accuracy is still an issue.

There is an open discussion about using time or crank angle based models for the NO_x prediction. For the case of pressure based models, crank angle sampling seems more logical as volume can be easily linked with pressure trace. However, these models require heavy calculations and big memory resources. The time required for completing one engine cycle is often bigger than the characteristic time of the engine. In order to overcome this limitation, some authors have proposed simplifications. Guardiola *et al.* [18] develop a semi-physical discrete event model based on the heat release calculation but considering only one zone as the main contributor to the NO_x formation; the process is supposed adiabatic, approaching T_f with the adiabatic temperature of the process. This approach requires specific corrections, especially when the combustion temperature is low. Other examples are Westlund and Åmströng [22] who present a fast physical model for NO_x and soot, or Arsie *et al.* [23] who present a hierarchical model structure for engine control design with different models and layers, ranging from physical based to mean value approaches. The latter examples might be named as semi-control oriented models.

2.1. Control-oriented models

For the sake of simplicity, control-oriented models might be divided into black box and grey box models. Black box models rely on system identification [24] and their quality is linked to the quality of the data used for training the model: the Design of Experiments (DoE) is not an easy task. Some examples are: Hirsch *et al.* [25] who present a gray box model for NO_x and PM, Takagi-Sugeno fuzzy models [26, 27], Hammerstein-Wiener (HW) [28], or Neural Networks (NN) [29, 30, 31, 32].

In commercial ECUs, the prevailing approach is to use look-up tables and curves to model non-linear and operating point dependent behaviours because of the simple programming: this structure gives the advantage to the engineer of linking the calibration of a certain parameter with a certain operating point or variations around it [33, 34]. Furthermore, OEMs have developed automatic procedures for filling the maps, curves and parameters from the ECU. However, this does not liberate from an intensive tuning effort in terms of number of parameters and required tests. These approaches might be described as grey-box approaches as they use first principle equations and calibratable parameters to get the outputs.

If comparing black and grey box structures, both approaches get similar predictive accuracies since they are dependent from the training data used for fitted the parameters. In this work, a grey box structure based on maps and first principle equations is preferred since it is consistent with the standard models in the ECUs and it permits the direct application of adaptive strategies for updating the parameters and the drift correction, as discussed in the part 2 of this paper. The

validity of this quasi-static representation for engine transients is an important factor to consider and it is assessed in the next subsection.

2.2. *Validity of a quasi-static model definition*

As commented before, the ECU-oriented models rely on static maps depending on the operating point conditions. This subsection discusses the validity of such definition for reproducing engine transients. For that, it is necessary to make reference to the engine control.

The engine works in closed loop by mainly controlling set-point references for air mass flow ($\dot{m}_a^*$) and boost pressure (p_{boost}^*), which are controlled by modifying the actuators for EGR (u_{egr}) and waste-gate (u_{wg}) -or variable geometry turbine alternatively-. Other variables such as the coolant temperature (T_{cool}) are also measured and taken into account in the ECU controller. Speed (n) and injection (m_f) are used as scheduling variables in order to build the references for the controllers by means of look-up tables. Since fuel path control representative times are in the order of μs, they can be considered as instantaneous if compared with air path dynamics. However, the major influence of the air path over the fuel path is with the smoke limiter, which limits the injected fuel rate until $\dot{m}_a$ or p_{boost} (depending on the manufacturer) reach a certain limit in order to bound λ^{-1}. Therefore, the engine states (X) might be modelled with the dynamic equation

$$\dot{X} = f(X, n, m_f, u_{\text{egr}}, u_{\text{wg}}, T_{cool}) \tag{3}$$

The set-point references for air and boost pressure ($\dot{m}_a^*$ and p_{boost}^*) are modelled by look-up tables scheduled by n and m_f

$$\dot{m}_a^* = f(n, m_f) \tag{4a}$$

$$p_{boost}^* = f(n, m_f) \tag{4b}$$

The variables $\dot{m}_a$ and p_{boost} are measured by sensors in diesel production engines, and if considering them as fast signals and neglecting mass storage effects (MAF sensor for measuring $\dot{m}_a$ is usually installed upstream of the low pressure compressor), u_{egr} and u_{wg} are represented by their effects on $\dot{m}_a$ and p_{boost}

$$\dot{X} = f(X, n, m_f, \dot{m}_a, p_{boost}, T_{cool}) \tag{5}$$

If the engine air path states are modelled by quasi-static representations (dynamics do not have influence on the output) or by adding filters and delays function only of the scheduling inputs n and m_f, then the dependency with $\dot{m}_a$ and p_{boost} might also be modelled as function of n and m_f.

The influence of the thermal effects over the engine is quite more complicated. On one hand, T_{cool} is the coolant temperature and it estimates the engine block temperature. This measurement is used in the engine in order to select the cold or warm engine strategies. The ECU usually has different maps for the injection settings depending on T_{cool}, e.g. when the engine is warm, the start of injection is forwarded or the number of injections might be different with respect to the warm strategies. The smart solution for modelling the engine states is maintaining this strategy and fit different maps at different temperatures: at cold start when $T_{cool} < 30$°C, at warm-up phase when 30°C$< T_{cool} <$ 60°C, and at normal operation when T_{cool} is around 90°C, values that depend on the considered engine. In addition, small variations of T_{cool}, even though when not affecting a change of mode, i.e. when T_{cool} varies between 75 and 90 °C, will also affect the engine operation, especially the combustion and should be considered in a model as well.

However, T_{cool} only measures the coolant temperature, but its resolution is not sufficient to represent the in-cylinder conditions. The temperature of the cylinder walls deserves a specific consideration, and its influence over the NO_x emissions is discussed latter in this work.

Based upon this reasoning, the state X might be represented as

$$\dot{X} = f(X, n, m_f, T_{cool}) \tag{6}$$

where the T_{cool} should be used in order to select the mode operation (the proper selection of operating point dependent maps) and also for considering its influence around the selected mode.

Putting aside the thermal dynamic effects and considering that the engine runs already warm, further simplifications could be made if the engine variations are slow enough that $\dot{m}_a$ and p_{boost} are able to track $\dot{m}^*_a$ and p^*_{boost} fast. In that case, the engine modelling could be further simplified to

$$X = f(n, m_f) \tag{7}$$

Figure 1 shows examples of the set-point references and responses for the air and fuel path and for three different cycles (see Section 5 for a description of the engine and Appendix D for a description of the cycles NEDC, CADC and SDMP), including also in the bottom plots the variables u_{egr} and u_{wg} corresponding to the actuation signals for EGR and WG respectively. The cycles correspond in that order from the slowest to the fastest transients. In the NEDC test, the air path controllers track with a minimum error both $\dot{m}^*_a$ and p^*_{boost}, especially for the case of $\dot{m}_a$ which is logical due to the slower dynamics associated to the turbo inertia. The response for the CADC is also good but transients are a little bit more aggressive than for NEDC, and the errors are slightly higher. For these two cycles, the quasi-static representation defined by (7) gives good results if the engine is already warmed up (T_{cool} is stable). However, for the case of SDMP cycle, the transients are much more aggressive and errors on the $\dot{m}_a$ and p_{boost} tracking are appreciable as well as the fact that the EGR valve is mostly closed during the cycle and the bi-turbo mode of the considered engine is indeed working at some points (see Figure 1). For this cycle, the engine is running at conditions different to the base calibration ($\dot{m}^*_a$ and p^*_{boost} are different from the other cycles) and the effect of the thermal loading due to the fast transients is critical.

Thus, the selection of the model structure for a given precision would not depend only on the engine characteristics but on the use cases. In all these cases and examples, it should be considered not only the thermal transient effects but the sensor dynamics. Therefore, (7) should consider the sensor model if the output is compared with a sensor output. The model structure proposed in this paper, aimed to be representative of the engine performance under different conditions, is built on the basis of (5) as a quasi-static model representation and a dynamic equation for representing sensor dynamics:

$$X = f(n, m_f, \dot{m}_a, p_{boost}, T_{cool}) \tag{8a}$$

$$\dot{X} = f(X, t - \tau) \tag{8b}$$

where t is the time and τ the sensor delay. Furthermore, the model is calibrated and validated for an engine running in warm condition, provided that a multi-mode fitting could be made if aimed to get accurate results when the engine is cold.

3. Intake oxygen estimation

To the interest of developing a RT model for NO_x, the Arrhenius equation (2) can be arranged with two operating point dependent factors C_1 and C_2

$$\frac{d\text{NO}_\text{x}}{dt} = C_1 e^{-C_2/T} \tag{9}$$

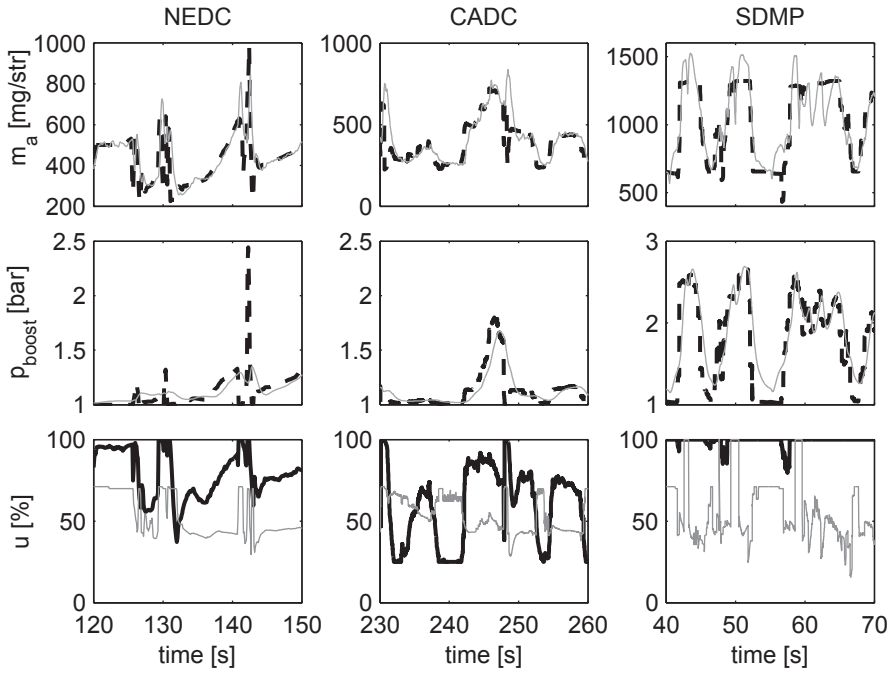

Figure 1: Air and fuel path response to variations in driver's command u_α for different cycles. First and second row plots: - - - is set-point $\dot{m}_a^*$ and p_{boost}^*, and —— is measured value of $\dot{m}_a$ and p_{boost}. Last row plots: —— u_{wg} [%], —— u_{egr} [%] is the smoke limit for injection. Note that 100% in u_{egr} corresponds to EGR valve fully closed and around 25% fully opened. For the case of u_{wg}, 100% corresponds to WG fully closed.

where C_1 includes gas intake concentrations (nitrogen and oxygen) while C_2 is the exponential factor. According to [7], oxygen rate in the cylinder and operating conditions (n and m_f as discussed above) seem to be suitable variables for predicting NO_x emissions. Hence it is possible to find a new generic expression whose structure is equivalent to 9:

$$x_{\text{NO}_x} = f([O_2]_{int}, x_1, ..., x_n) \tag{10}$$

where x_{NO_x} is the model output. This expression relates NO_x with $[O_2]_{int}$ and different parameters $(x_1, ..., x_n)$ including temperature and time reactions effects.

Figure 2 shows NO_x versus $[CO_2]_{int}$ in the intake manifold when varying EGR valve position for different speed n and injected fuel rate m_f. NO_x is normalised by $NO_{x,EGR=0}$, which corresponds to maximum value at every operating point (equivalent to EGR valve fully closed $u_{\text{egr}} = 0$). The exponential fit in Figure 2 is clear, in spite of operating point dependency of the exponential factor is not modelled yet.

In the following, the use of sensors and a simple model is discussed in order to estimate the intake oxygen.

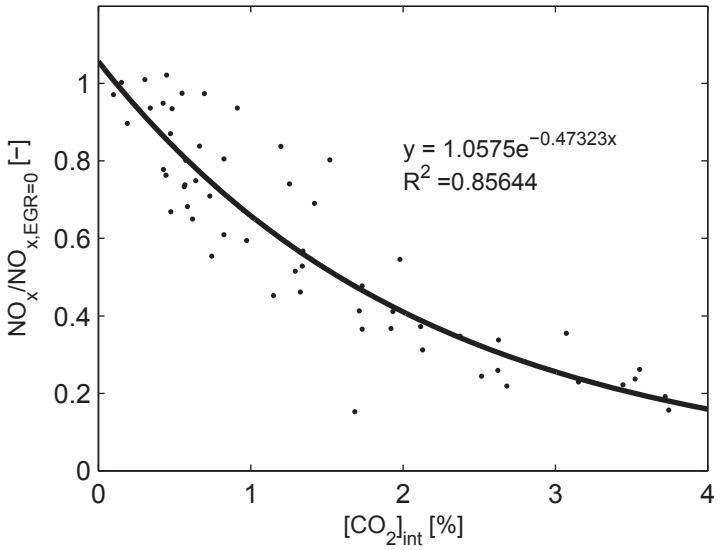

Figure 2: Normalised NO_x emissions as function of $[CO_2]_{int}$ for 37 operating points. Engine calibration is the standard given by the manufacturer.

3.1. Sensor approach

Due to the strong dependency of NO_x emissions on $[O_2]_{int}$, its measurement is of major importance. However, the lack homogeneity of the intake mix stands a major problem in some engines. In this work the methodology presented in [35] has been used for analysing the homogeneity of the mix. The method is based on feeding the gas analyser from different probes, as sketched in Figure 3:

- Measurement of the $[CO_2]_{int}$ just before the separation of the manifolds at the intake by the gas analyser,
- extractions in the four individual cylinder intake runners and measurement by the gas analyser (cylinder 1 to 4 $[CO_2]_{int}$ independent measurements),
- measurement of a sample result of the mix of the 4 extractions and made by the gas analyser (1 measurement, from a rail where gas coming from all the probes is mixed).

When using the gas analyser, the $[CO_2]_{int}$ [%] is measured with a non-dispersive infra-red method (NDIR). As the intake gas is a mix of ambient air and the results of the combustion of this air with fuel, the $[O_2]_{int}$ is linearly correlated with the $[CO_2]_{int}$ (the higher the $[CO_2]_{int}$, the lower the $[O_2]_{int}$).

Additionally, and as a real time alternative, the measurement of the intake λ by means of the UEGO sensor located in the intake manifold has been implemented. The sensor has been located with a certain distance upstream of the separation between individual cylinder runners for avoiding separation effects (1 measurement).

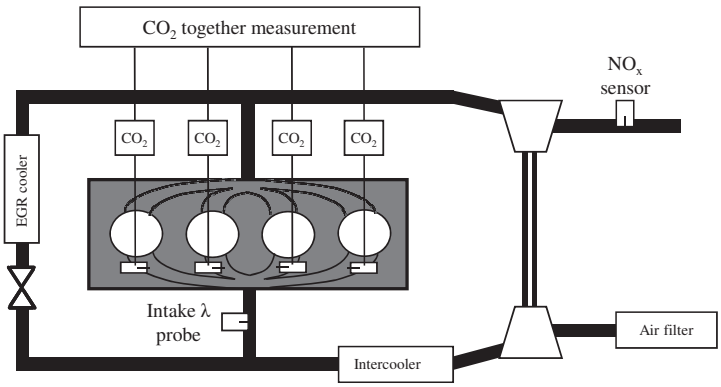

Figure 3: Engine layout showing the main sensors used for measuring $[O_2]_{int}$ or equivalently $[CO_2]_{int}$.

Operating point $[n, m_f]$	[2500, 35]	[2500, 7]	[1500, 20]	[1500, 7]
$[CO_2]_{int}$ intake [%]	1.37	1.07	1.27	2.30
$[CO_2]_{int}$ man.1 [%]	1.14	0.98	2.38	2.62
$[CO_2]_{int}$ man.2 [%]	1.65	1.09	2.46	2.92
$[CO_2]_{int}$ man.3 [%]	2.07	1.11	1.89	2.64
$[CO_2]_{int}$ man.4 [%]	1.89	1.10	1.79	2.55
$[CO_2]_{int}$ man. 1-4 [%]	1.62	1.07	2.27	2.73
$[CO_2]_{int}$ mean 1-4 [%]	1.69	1.07	2.13	2.68
std 1-4 [%]	0.40	0.06	0.34	0.16
$[CO_2]_{int}$ lambda [%] from I_p	1.99	0.95	2.10	2.80

Table 1: Comparison of different sensor outputs for determining the effective intake $[CO_2]_{int}$ (and thus $[O_2]_{int}$ and λ^{-1}) in the cylinder. The first row represents the measurement of $[CO_2]_{int}$ by a gas analyser just upstream of the manifolds at the intake junction; the rows 2-5 represent the gas analyser measurements of $[CO_2]_{int}$ by means of the 4 individual extractions of gas at the intake manifolds of the engine; the row 6 is the gas analyser measurement of the sample result of a mix of 4 equal extractions of the intake manifolds of each cylinder; rows 7-8 represents the mean and standard deviation of the 4 individual extractions of the gas measured in rows 2-5; while the last row represents the measurement of the intake lambda sensor after converting the I_p output to actual $[CO_2]_{int}$ (see Figure 4).

UEGO sensor provides the ion pump current I_p [mA]. The I_p signal is previously corrected with the effect of p_{boost} which affects to the oxygen partial pressure measurement. Furthermore, I_p is related with λ^{-1} (and thus $[O_2]_{int}$ and $[CO_2]_{int}$) by a curve given by the manufacturer.

A set of measurements is made in order to evaluate the different alternatives and to determine the best method to estimate intake gas concentration. In total 4 operating points $[n\ m_f]$ are studied: [2500,35], [2500,7], [1500,20] and [1500,7] (units are rpm and mg/str respectively) with the rest of inputs fixed by the standard engine calibrations.

The results of the study are summarised in Table 1 for the 4 operating points. Even though there exists important dispersion among cylinder samples (due to not utilizing a mixer that guarantees the homogeneity of the fluid at intake), the comparison of the mean value for the 4 cylinders with the measurement from the rail (Cyl 1-4 probe) is satisfactory. Nevertheless, the $[CO_2]_{int}$ measured just before the cylinder manifolds is highly affected by the lack of homogeneity in the mix and the signal presents a significant error when compared with the rest of alternatives. The

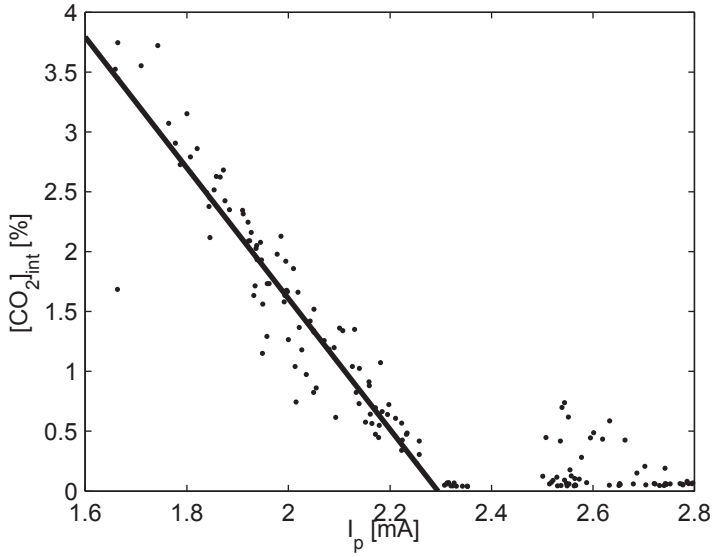

Figure 4: Equivalency between $[CO_2]_{int}$ and I_p corrected by pressure. The saturation of the intake probe is evident in both plots when I_p reaches around 2.3, i.e. equivalent to low $[CO_2]_{int}$ values

results obtained by the UEGO sensor are acceptable, despite of a slight deviation lower than that of the gas analyser intake extraction. However, the resolution of the intake lambda probe presents a saturation when $I_p > 2.3$ mA (low $[CO_2]_{int}$ and high $[O_2]_{int}$) as shown in Figure 4.

Intake lambda sensors could be installed for estimating intake oxygen, but a model based estimation is proposed here. Anyway, if an intake lambda probe is installed, an observer may be designed for improving the estimation.

3.2. Model approach

$[O_2]_{int}$ can be measured, but intake lambda probes are not always available in diesel engine production cars, and measurements errors related with the gas non-homogeneity may appear [35, 4]. As commented before, UEGO sensors could also be used for measuring intake oxygen. However, important problems linked with the pressure effects over the output signal, which drive to saturation and the need of compensation, can distort the signal. In those cases and if the sensor is presented, estimation theory is a good solution.

Alternatively, $[O_2]_{int}$ can be modelled by relating $[O_2]_{int}$, EGR and λ^{-1}

$$[O_2]_{air}(1 - \lambda^{-1}) = [O_2]_{exh} \tag{11}$$

By the oxygen balance at the intake junction

$$[O_2]_{int} = [O_2]_{air}(1 - EGR) + [O_2]_{exh}EGR \tag{12}$$

and substituting the former in the latter

$$[O_2]_{int} = [O_2]_{air}(1 - EGR\lambda^{-1}) \tag{13}$$

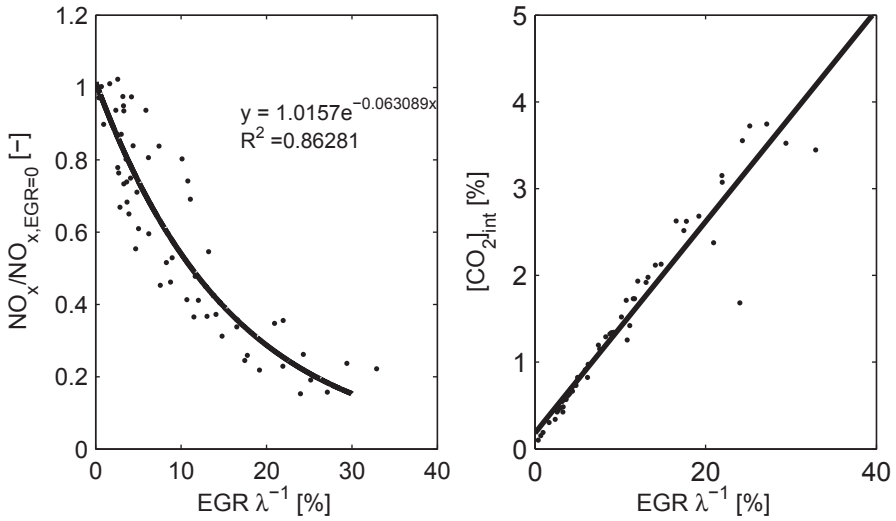

Figure 5: Left plot shows normalised NO_x emissions as function of $EGR\lambda^{-1}$ for 37 operating points in the diesel engine. Right plot shows the fitting of $[CO_2]_{int}$ and $EGR\lambda^{-1}$ with a good agreement.

that shows a direct relationship between $[O_2]_{int}$ and $EGR\lambda^{-1}$. The product $EGR\lambda^{-1}$ is often called the inert gas rate and represents the actual portion of exhaust gas that has reacted with the injected fuel and then contains no available oxygen; e.g Andersson *et al.* [36] use $EGR\lambda^{-1}$ for designing a fast NO_x model. Figure 5 shows the NO_x fitting with $EGR\lambda^{-1}$ and the fitting between $EGR\lambda^{-1}$ and $[CO_2]_{int}$, where the expression (13) is proved.

On the other hand, Figure 6 shows the fitting of NO_x by using EGR. Results with EGR are much worse than with $EGR\lambda^{-1}$ and is difficult finding a tendency, which proves that $EGR\lambda^{-1}$ seems a good alternative for estimating $[O_2]_{int}$ (or $[CO_2]_{int}$) when an intake lambda probe is not installed, although uncertainty propagation from the different involved measurements is to be checked [4]. Afterwards, Table 3 shows the results of using the different possibilities (sensors and models) for estimating the $[O_2]_{int}$. Based on the discussions of this section, the NO_x model is presented in the next.

4. Real Time NO_x model

An ECU-oriented NO_x model is designed by a set-point relative structure, where maps are used for reproducing nominal NO_x emissions, while the effect of the intake oxygen is captured by an exponential variation. Other effects, including the thermal loading, the humidity or the intake mass flow dependency, are modelled by tabulated factors. By using this modelling approach, it is assumed that there are no interactions between the inputs and each act independently on the NO_x formation process.

The following hypotheses are assumed:

- Model is programmed and calibrated in discrete form and frequency used for simulation is 50 Hz.

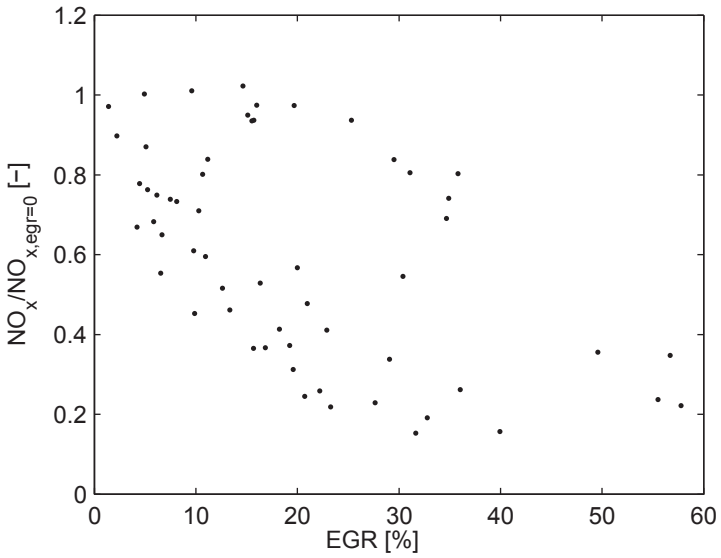

Figure 6: Normalised NO_x emissions as function of *EGR* for 37 nominal operating points for the DW12B engine

- Model is based on a set of static look-up tables, curves and parameters with the addition of discrete filters and lag blocks in order to consider system dynamics.
- Intake conditions ($\dot{m}_{int}$ and T_{int}) are calculated on the basis of the volumetric efficiency and an EGR flow model by assuming constant pressures upstream and downstream of the intake junction and a mixing model for the temperature.
- Engine combustion is tabulated by using look-up tables related to nominal conditions and variations of the intake conditions.
- EGR path is modelled with a cooler model and a filter for accounting manifold dynamics.
- Turbocharger effects are bypassed by directly using sensor signals from $\dot{m}_a$ and p_{boost}. The former located upstream of the compressor and the latter downstream of the intercooler.
- The model results and validation are considered for warm engine operation, i.e. the coolant temperature (or engine block temperature) measured by the ECU is around 80-90 °C. However, small variations around this value are taken into account, considering that higher variations could lead to the engine to change the injection settings. For those cases, a multi-mode map programming is advisable. This is not considered in this work.

The model scheme is outlined in Figure 7. In the top right and for clarifying the reader, engine positions subscripts are shown: *boost* is downstream the intercooler, *int* the intake manifold, *egr* the EGR manifold at the intake junction and *exh* the exhaust. The main RT NO_x model requires two additional blocks: a mean value engine calculation of the EGR flow for obtaining *EGR* and the calculation of the fuel-to-air ratio λ^{-1}. The model design is flexible and other structures for

the EGR flow and λ^{-1} model or measurement might be utilised just replacing the corresponding blocks.

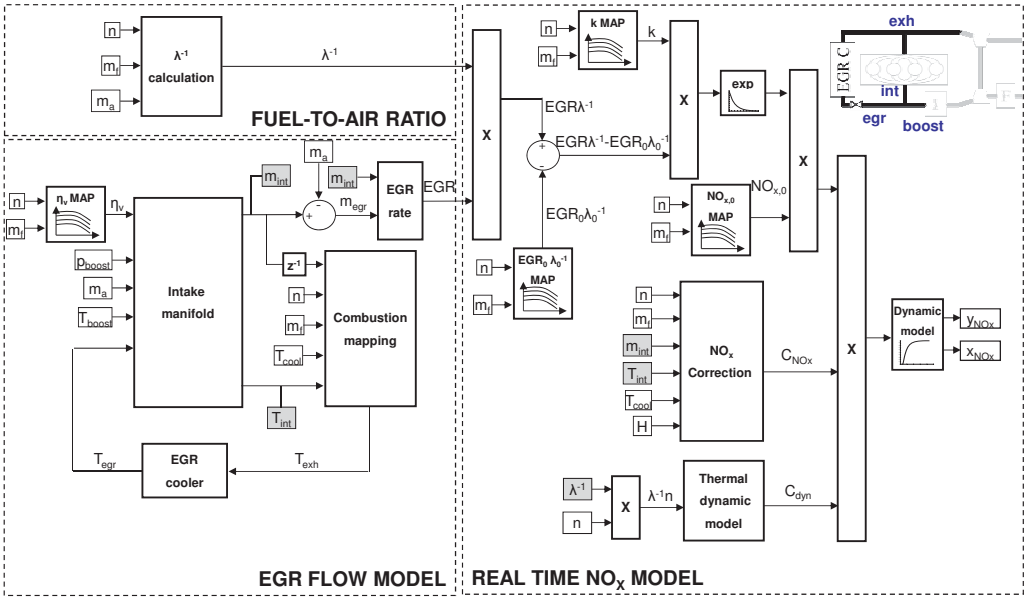

Figure 7: Structure of the RT NO_x model, where the main blocks are depicted: the EGR flow model (or air path model), the fuel-to-air ratio calculation and the proper NO_x model calculation. The model inputs (coming from ECU signals) are marked with squares with white front, while the squares with gray front are used as short-cuts for linking intermediate variables in the model. At the top right, the legend for the engine positions is shown.

The state vector X for the model is built as

$$X = \begin{bmatrix} x_{\mathrm{NO_x}} & y_{\mathrm{NO_x}} & C_{dyn} \end{bmatrix}^T \tag{14}$$

where $x_{\mathrm{NO_x}}$ is the NO_x model output (actual NO_x), $y_{\mathrm{NO_x}}$ is the filtered and delayed NO_x output (for comparing with NO_x sensor) and C_{dyn} is a dynamic factor for coping with in-cylinder temperature and explained bellow. The input signals contained in the vector U are available in the ECU and are shown in squares in the Figure 7

$$U = \begin{bmatrix} n & m_{\,f} & p_{boost} & \dot{m}_{\,a} & T_{boost} & T_{cool} & H \end{bmatrix}^T \tag{15}$$

where H is the humidity and the rest of variables have already been defined. Model output vector Y is the modelled sensor response

$$Y = y_{\mathrm{NO_x}} \tag{16}$$

in order to have a comparable signal with NO_x sensor output during dynamic tests. $x_{\mathrm{NO_x}}$ indicates the raw or actual NO_x, which must be filtered and delayed. A delayed first order discrete model is used

$$y_{\mathrm{NO_x}} = \mathrm{z}^{-\tau_{\mathrm{NO_x}}} \frac{1 - a_{\mathrm{NO_x}}}{1 - a_{\mathrm{NO_x}} \mathrm{z}^{-1}} x_{\mathrm{NO_x}} \tag{17}$$

where $a_{\mathrm{NO_x}}$ is the sensor time response and $\tau_{\mathrm{NO_x}}$ is the total sensor delay; see [37] for a full method on NO_x sensor output characterisation.

4.1. NO_x calculation

The exhaust NO_x emissions are calculated in (18) and consists in a single function refer-enced to conditions with nominal EGR for calculating x_{NO_x}, which is affected by an exponential $EGR\lambda^{-1}$ correction and additional factors C_{NO_x} and C_{dyn}. This structure guarantees that nominal test corrections are eliminated minimising the nominal error and subscript 0 goes with nominal conditions. Then, the model x_{NO_x} output is calculated as follows

$$x_{NO_x} = NO_{x,0} \cdot e^{-k_{NO_x} \cdot (EGR\lambda^{-1} - EGR_0\lambda_0^{-1})} \cdot C_{NO_x} \cdot C_{dyn} \tag{18a}$$

$$C_{NO_x} = C_{\dot{m}_{int}} \cdot C_{T_{int}} \cdot C_{T_{cool}} \cdot C_h \tag{18b}$$

where C_{NO_x} and C_{dyn} are used as correction factors to the model structure, and are explained in subsequent paragraphs.

4.1.1. Correction factors

C_{NO_x} is calculated on the basis of previous experience and tests made in the engine (see [38] for a sensitivity study of NO_x to relevant engine inputs). For that, 4 important effects are included in C_{NO_x}: (19a) $C_{\dot{m}_{int}}$ indicates variations of intake mass flow $\dot{m}_{int}$ [35]; (19b) $C_{T_{int}}$ copes with intake temperature T_{int}; (19c) $C_{T_{cool}}$ relates engine temperature (especially for coping with small variations around the nominal engine coolant temperature [39]); (19d) C_h considers Humidity H (if a humidity sensor is available). Expected NO_x sensitivity for the different parameters is depicted at the right side of (19). $k_{\dot{m}_{int}}$, $k_{T_{int}}$, $k_{T_{cool}}$, k_h are calibrated by [n,m_f] dependent maps. If engine is operating at nominal conditions then $C_{\dot{m}_{int}}, C_{T_{int}}, C_{T_{cool}} = 1$. Equations are shown in the following.

$$C_{\dot{m}_{int}} = 1 + k_{\dot{m}_{int}} (\dot{m}_{int}/\dot{m}_{int,0} - 1) \qquad \uparrow \dot{m}_{int} \downarrow NO_x \text{ [1]} \tag{19a}$$

$$C_{T_{int}} = 1 + k_{T_{int}} (T_{int}/T_{int,0} - 1) \qquad \uparrow T_{int} \uparrow NO_x \tag{19b}$$

$$C_{T_{cool}} = 1 + k_{T_{cool}} (T_{cool}/T_{cool,0} - 1) \qquad \downarrow T_{cool} \downarrow NO_x \tag{19c}$$

$$C_h = 1 + k_h H/0.03 \qquad \uparrow H \downarrow NO_x \text{ [2]} \tag{19d}$$

4.1.2. Thermal loading model

T_{cool} is usually measured on-board and is the engine coolant temperature. This temperature is the only indirect reference to the temperature of the engine block. T_{cool} is used on-board in order to define engine modes, i.e. the models in the ECU can have maps or parameters calibrated at different engine temperatures. According to the T_{cool} measurement, the ECU is able to select the appropriate mode at every moment. For instance, when the engine is cold, the injection is forwarded in order to warm-up the engine.

In series diesel engines, neither the engine block temperature nor the in-cylinder temperature (T_{cyl}) are measured on-board (and rarely in test benches) and they are factors of great importance

[1] If p^*_{boost} set-point is increased for a constant air mass flow ($\dot{m}_a$) set-point, then u_{egr} will be opened and more $\dot{m}_{egr}$ will enter the cylinder (consequently $\dot{m}_{int}$ will be higher), producing that NO_x should be lower. This effect can be shifted if u_{egr} is already opened, especially at low load and regime areas, or engine is running out of EGR area.

[2] Moisture increases air specific heat c_p, diminishing in-cylinder temperature T_{cyl}.

for NO_x formation in diesel engines. However, the reproducibility of these temperatures by only using T_{cool} is not clear at all conditions.

For example, if the engine is in steady-state operation, T_{cyl} might be approximated as function only of the operating point conditions, and then T_{cool} is used in order to select the appropriate mode (T_{cool} permits to switch among the different mode dependent maps)

$$T_{cyl} = f(T_{cool}, n, m_f) \tag{20}$$

but if the engine is in transient operation, e.g. a tip-in from idle or low loads, it is necessary to consider an extra degree-of-freedom since T_{cyl} will be related with the history of the engine load. For this case, the measurement by T_{cool} itself is not capable of representing the actual value of T_{cyl}. Furthermore, T_{cool} is also controlled by the ECU in closed loop to keep a constant value between 80-90°C. Therefore and for those cases

$$T_{cyl} \neq f(T_{cool}, n, m_f) \tag{21}$$

There exists the possibility of installing a temperature sensor at the exhaust but even though this option should be interesting for improving the model accuracy, these sensors are not usually available on-board. Alternatively, a 0-Dimensional approach may consider the heat conductive problem between the cylinder temperature and the coolant. According to that, the released heat power ($\dot{Q}$) might be linked with the in-cylinder temperature variation (ΔT_{cyl})

$$\dot{Q} \propto \Delta T_{cyl} \tag{22}$$

The total heat dissipation (Q) between the cylinder and the coolant depends on ΔT_{cyl} and the considered time, which is inversely proportional to n. At the same time, the heat dissipation will also be linked to the combustion efficiency and thus λ^{-1}

$$\lambda^{-1} = \Delta T_{cyl} \frac{1}{n} \tag{23a}$$

$$\Delta T_{cyl} \propto \lambda^{-1} n \tag{23b}$$

which shows that $\lambda^{-1}n$ is related with the thermal load in the cylinder and could be used as an estimator for the problem.

A multiplicative factor C_{dyn} to the NO_x model output is proposed. This factor augments the state vector X and gives some correction regarding the T_{cyl} variation. The correction factor is designed for correcting the NO_x output only during transient, since steady state effects due to changes in T_{cool} are yet corrected through $C_{T_{cool}}$. The main equation is presented in (24) and the Figure 8 shows the scheme of the function. C_{dyn} is built with the filtered difference of $\lambda^{-1}n$, which represents the engine thermal load variation (other options have also been checked, but this has given the best results for the model, which is in line with the discussion above), and a calibrated gain k_{dyn}. When the engine runs in steady-state operation, so $\lambda^{-1}n$ is, $C_{dyn} = 1$. In addition, this factor is set to one for steady-state simulations.

$$C_{dyn} = 1 + k_{dyn} \cdot (\lambda^{-1} n) \left(1 - z^{-\tau_{dyn}} \frac{1 - a_{dyn}}{1 - a_{dyn} z^{-1}}\right) \tag{24}$$

Figure 9 shows relevant signals during a sharp engine transient in n and m_f. T_{exh} is measured with a sensor and compared with T_{cool} showing two effects: First, T_{cool} is much more filtered and

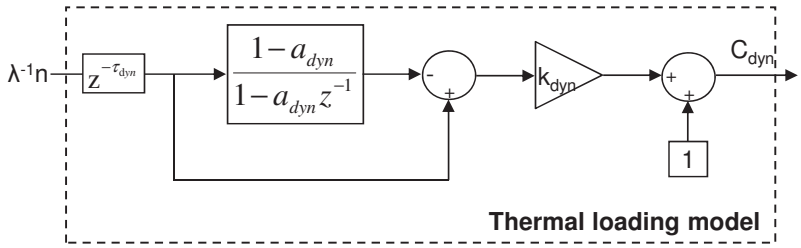

Figure 8: Block diagram of thermal loading factor C_{dyn}

delayed than T_{exh}, and second, the sensitivity of T_{cool} is not sufficient for representing the actual thermal transient occurring on-engine, i.e. T_{cool} hardly varies from 82 to 92 °C while T_{exh} goes from 200 to 700 °C. Bottom plot shows the value C_{dyn} tuned for the NO_x model, being lower than 1 during the transient but finally converging to 1. This is for representing that engine comes from a colder state. In that plot, NO_x sensor (z_{NO_x}) is compared with y_{NO_x} model output (see (17)) without C_{dyn} (it overestimates NO_x) and with C_{dyn}.

4.2. EGR flow model

The EGR rate

$$EGR = \frac{\dot{m}_{egr}}{\dot{m}_{int}} \tag{25}$$

is calculated on the basis of a mean value model of the volumetric efficiency (η_v) using boost pressure (p_{boost}) and air mass flow ($\dot{m}_a$) inputs coming from commercial sensors. The model block diagram is shown in Figure 10.

The intake manifold mass flow ($\dot{m}_{int}$) is obtained from η_v (mapped with the steady-state tests). p_{boost} is assumed constant in the manifolds that confluence at the intake (*egr*,*boost*,*int*) while T_{boost} is measured and T_{int} calculated by means of a combustion model based on maps and corrections over T_{cool} and $\dot{m}_{int}$.

$$\dot{m}_{int} = \frac{\eta_v \, n_{cyl} \, V_d \, n \, p_{boost}}{2 \, R \, T_{int}} \tag{26a}$$

n, m_f, T_{boost} and $\dot{m}_a$ are measured by sensors, the unit displaced volume (V_d) and the number of cylinders (n_{cyl}) are known beforehand and a model is proposed for T_{int}. For instance, Wahlström *et al.* [40] propose an isothermal model ($T_{int} = T_{boost}$); for the current work a mixing model based on energy conservation at the intake junction is utilised, i.e. intake volume is small and mixing is so fast that no heat is transferred to the walls. Therefore and assuming that the specific heat capacities are equal for all gases,

$$\dot{m}_{int} T_{int} = \dot{m}_a T_{boost} + \dot{m}_{egr} T_{egr} \tag{27}$$

and from (26), the product $\dot{m}_{int} T_{int}$, which defines the intake enthalpy flow, can be inferred as

$$\dot{m}_{int} T_{int} = \frac{\eta_v \, n_{cyl} \, V_d \, n \, p_{boost}}{2R} \tag{28}$$

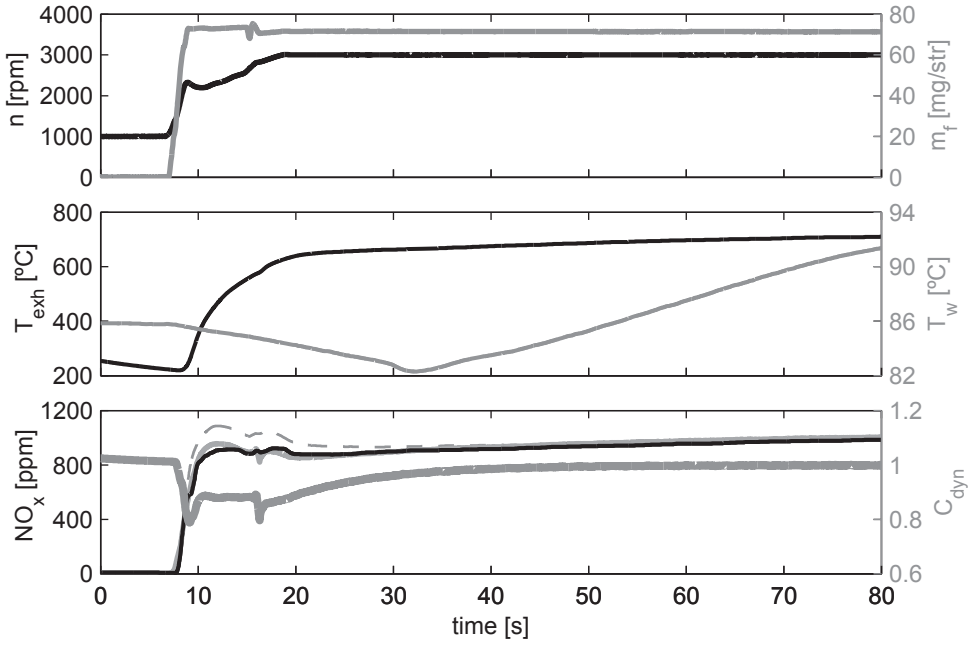

Figure 9: NO_x and thermal response during a sharp transient. Top plot: n and m_f evolution. Middle plot: Exhaust temperature T_{exh} and coolant temperature T_{cool} during the transient. Dynamics of both signals, especially for T_{cool}, are slow, which affects final NO_x. Bottom plot and left axis: —— z_{NO_x} by sensor, - - - y_{NO_x} with $C_{dyn} = 1$, —— y_{NO_x} using C_{dyn}. Bottom plot and right axis: ▬ C_{dyn} factor calculated by thermal model.

and rewriting the mass equilibrium at the intake junction

$$\dot{m}_{egr} = \frac{\eta_v \, n_{cyl} \, V_d \, n \, p_{boost}}{2RT_{int}} - \dot{m}_a \tag{29}$$

and finally substituting in (27), T_{int} can be solved

$$T_{int} = \frac{\eta_v \, n_{cyl} \, V_d \, n \, p_{boost} \, T_{egr}}{\eta_v \, n_{cyl} \, V_d \, n \, p_{boost} + 2 \, R \, m_{boost} \left(T_{egr} - T_{boost} \right)} \tag{30}$$

Two additional models (see Figure 10) are needed in order to calculate T_{egr} (not usually measured on commercial engines): a T_{exh} model and an EGR cooler efficiency model.

4.2.1. T_{exh} model

Temperature increase between the intake and the exhaust ΔT_{ie} is calculated from a map and corrections

$$T_{exh} = T_{int} z^{-1} + \Delta T_{ie} \tag{31}$$

adding the delay z^{-1} for coping with causality.

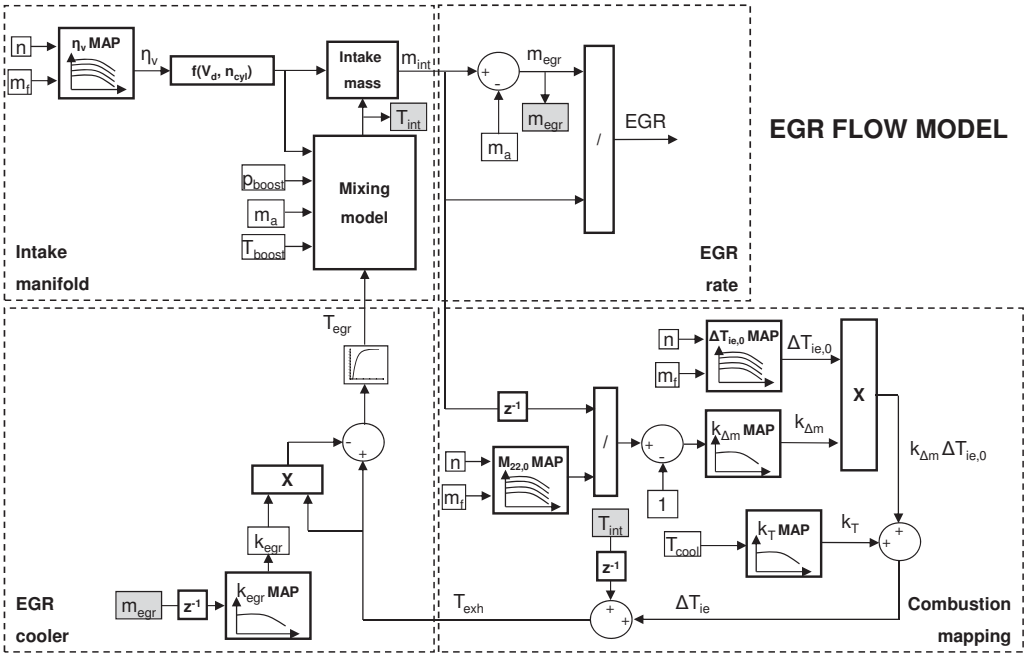

Figure 10: Structure of the EGR flow model

ΔT_{ie} can be calculated on the basis of heat release functions (e.g. Wiebe for Watson functions) and solving the principle equations of the cylinder, or fitted to experimental values. Since the results of such physical approach may be calculated beforehand, a map based model coherent with the full RT NO_x model is proposed with two corrections based on $\dot{m}_{int}$ and T_{cool}

$$\Delta T_{ie} = \Delta T_{ie,0} \cdot k_{\Delta m} + k_T \tag{32}$$

Maps depending on $[n, m_f]$ are used for generating references for $\Delta T_{ie,0}$ and $\dot{m}_{int,0}$. Then Δm is calculated

$$\Delta m = \frac{\dot{m}_{int} z^{-1}}{\dot{m}_{int,0}} - 1 \tag{33}$$

and defining the calibrated map output

$$k_{\Delta m} = f(\Delta m) \tag{34}$$

The engine block temperature also affects the final NO_x emissions, and in the context of the previous discussion about C_{dyn}, T_{cool} may be used here to get the effect of minor variations in T_{cool}, which represents variations in the engine block temperature. This factor is calculated from the curve

$$k_T = f(T_{cool})$$

Alternatively, the dynamic component of temperature rise due to combustion is considered with the aforementioned C_{dyn} factor and is directly affecting the final NO_x emissions.

The effect of injection parameters. Injection duration (t_{mi}), start of injection (SOI) and common rail pressure (p_{rail}) affects heavily the in-cylinder temperature and thus NO_x emissions [41]; and so is the engine speed (n) that is coupled with the others, but here considered as an input for the model. In this work and as stated in the model hypotheses, the injection settings from the series calibration are maintained. Therefore, t_{mi}, SOI and p_{rail} are completely defined by the operating point conditions, i.e. every pair [n, m_f] defines a nominal value for these variables.

However, extra maps for covering variations over the SOI or p_{rail} might be considered, making possible the use of the model for the injection control. This correction might update the combustion model by including the parameters k_{SOI} and $k_{p_{rail}}$, modifying (32) as follows

$$\Delta T_{ie} = \Delta\, T_{ie,0} \cdot k_{\Delta m} \cdot k_{SOI} \cdot k_{p_{rail}} + k_T \tag{35}$$

These factors are advisable in such cases, but they have not been calibrated in the scope of this work, since the injection settings defined by the series calibration have been applied in all tests.

4.2.2. EGR cooler model

T_{egr} is calculated by a temperature drop and a first order discrete filter with time response a_{egr} and a transport delay τ_{egr}

$$T_{egr} = z^{-\tau_{egr}} \frac{1 - a_{egr}}{1 - a_{egr} z^{-1}} \left(T_{exh} - k_{egr} (T_{exh} - T_{cool}) \right) \tag{36}$$

where k_{egr} is calculated by the curve

$$k_{egr} = f(\dot{m}_{egr}) \tag{37}$$

and τ_{egr} is function of the engine characteristic time

$$\tau_{egr} = \frac{k_{\tau_{egr}}}{n} \tag{38}$$

4.3. λ^{-1} model

Depending on the engine configuration, an air mass flow sensor ($\dot{m}_a$) may be present (or mass flow can be estimated through the boost pressure), and the injected fuel mass flow ($\dot{m}_f$) is usually estimated by the ECU. A simple model may be then proposed

$$x_{\lambda}^{-1} = 14.5 \frac{\dot{m}_f}{\dot{m}_a} \tag{39}$$

where $\dot{m}_f$ and $\dot{m}_a$ quantities are expressed in the same units, i.e. mg/str or kg/s, and 14.5 stands for the stoichiometric air-to-fuel ratio. Note that the model neglects the mass accumulation in the intake and exhaust manifolds. Despite such effects should be considered for correcting $\dot{m}_a$ during the engine transients (for example, when boost pressure is increased or when shifting between boosting modes [42]), they will be neglected hereinafter for simplicity. The reader is referenced to [43] for a complete methodology to model λ^{-1} and other interesting topics.

Stroke (S)	96 mm
Bore (D)	85 mm
S/D	1.129
Number of cylinders (z)	4
Displacement	2179 cm^3
Turbocharging system	Sequential parallel [44]
Valves by cylinder	4
Maximum power	125 kW@4000 rpm
Compression ratio	17:1

Table 2: Engine technical data.

5. Experimental Facility

Experimental data is obtained from a turbocharged diesel engine. This engine is a 2.2-liter 4-cylinder common rail whose specifications are shown in Table 2. The standard air cooler downstream the compressor is replaced by a water intercooler because of the lack of forced air flux. All after-treatment devices are removed, they are out of the scope of the paper.

This engine is installed on an engine test bench and coupled to a variable frequency eddy current dynamometer that allows carrying out dynamic tests. A rapid prototyping system is connected via ETK to a bypass-allowed ECU, permitting commanding and receiving signals by means of coupling a real time system via CAN. Besides the commercial sensors, a full set of sensors is installed in the engine measuring full operating conditions (pressure and temperature in the manifolds, mass flows, speed, torque, fuel consumption, etc.), atmospheric conditions (also humidity), emissions by a gas analyser [45] (NO_x, CO, CO_2, PM, etc.), and both NO_x and richness (λ^{-1}) by an on-board NO_x sensor. Some of them are measured twice, by software connected to ECU and test bench software. All sensors installed have previously been tested and calibrated with standard procedures, both in steady and transient-state.

Most of the variables are used for calibration but not necessary for model running. Figure 11 shows the recommended on-engine sensor set, i.e. the key sensors required online once the model is calibrated. These are used for inputs to the model, removing the need to observe some of the variables. The NO_x sensor is not really necessary and the RT model can be used for online NO_x prediction. Appendix B shows main variables used throughout the paper.

6. Results

This section presents the tuning methodology and results of the NO_x model.

6.1. Tuning methodology

The NO_x model fitting is separated into the static tuning for filling up all the maps and model parameters; and the dynamic tuning by fitting the dynamic factors, fine tuning and model validation.

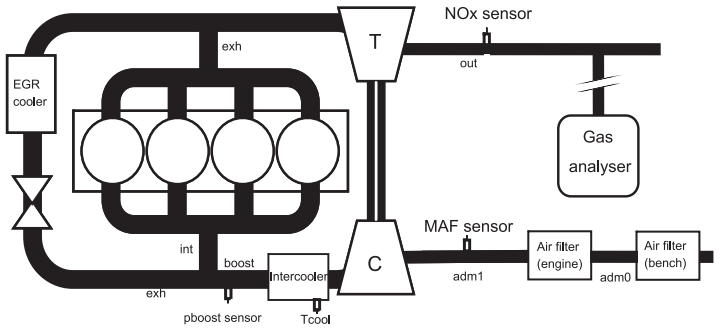

Figure 11: Engine commercial set recommended for the RT NO_x model.

Static tuning. A full set of steady-state tests are performed in order to characterise the engine and fit the tables and parameters of the model. This includes different pairs of $[n, m_f]$ values covering:

- nominal tests, defined by manufacturer ECU settings, with warm conditions and variables stabilised,
- variations of EGR rate,
- variations of engine coolant temperature (T_{cool}),
- variations of water temperature of the intercooler (T_{wic}) to influence T_{int}, and
- variations of p_{boost} to influence on $\dot{m}_{int}$.

Ranges are selected in order to produce appreciable NO_x variations but taking into account the limits for engine operation. 363 steady measurements are made in total. Covered engine areas are shown in Figure 12.

The calibration sequence is the following:

- From all tests, η_v, $\dot{m}_{egr}$ and temperatures differences are calculated and used for fitting the maps as function of engine speed and fuel
- From nominal tests, maps are built for $NO_{x,0}$, $EGR_0\lambda_0^{-1}$ and $T_{cool,0}$ as function of engine speed and fuel.
- From all tests, RT NO_x model is simulated in order to estimate the results for $\dot{m}_{int}$ and T_{int}. The results are used for identifying $\dot{m}_{int,0}$ and $T_{int,0}$.
- The ratios $\dot{m}_{int}/\dot{m}_{int,0}$, $T_{int}/T_{int,0}$ and $T_{cool}/T_{cool,0}$ are calculated from all tests.
- Curves k, k_m, $k_{T_{int}}$, $k_{T_{cool}}$ and k_h are fitted by LS of the main equation (18). This adjustment is made independently by using the steady-state data set. In addition to $EGR\lambda^{-1}$ and in order to compare results with other possibilities for estimating $[O_2]_{int}$, I_p from an intake UEGO sensor and $[CO_2]_{int}$ from the gas analyser are evaluated. The results are presented in Table 3. The best fit is for $[CO_2]_{int}$ but this is not available on-board, while it can be used for tuning and validation. Therefore, the minimum error is achieved with the variable $EGR\lambda^{-1}$, which is calculated by modeling and sensor signals.

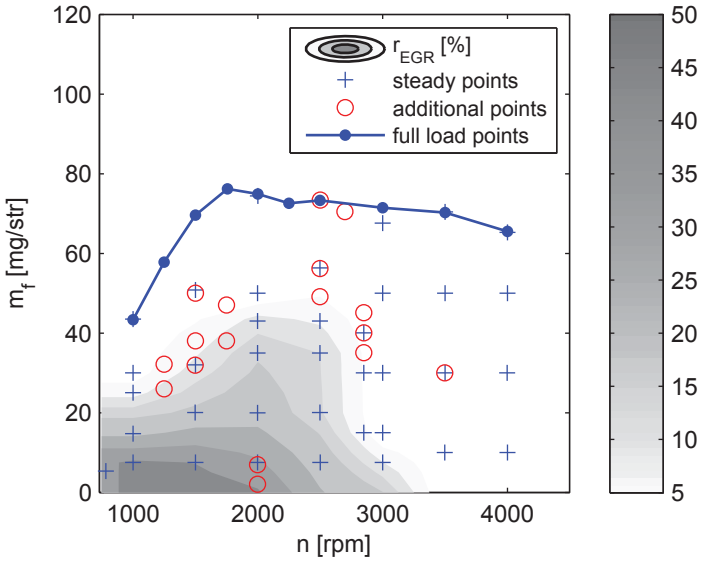

Figure 12: $[n, m_f]$ set of values run for testing the engine in steady-state. In each set, different variations of u_{egr}, T_{cool}, p_{boost} and T_{int} are made for characterizing the engine. Some additional points are measured for completing the engine characterization. Nominal EGR map EGR_0 (white area corresponds to EGR valve closed, $EGR = 0$) and full load line are also plotted.

	$EGR\lambda^{-1}$	Corrected Ip	$[CO_2]_{int}$ from gas analyser
g/h	9.31	9.78	8.54
%	8.09	8.96	7.58

Table 3: Mean errors when fitting the model with different input variables. $[CO_2]_{int}$ from the gas analyser is the mean of 4 extractions of the intake manifolds. $EGR\lambda^{-1}$ is calculated on the basis of the EGR mean value flow model and the λ^{-1} model. Signal from the intake lambda probe (I_p) is corrected by pressure and some data points with faulty measurements have been removed because they present problems with the sensor saturation. NO_x output is adjusted in g/h.

Dynamic tuning. Dynamic tests are used for adjusting the C_{dyn} factor parameters and for fine tuning of the maps and curves fitted with the steady-state tests. These dynamic tests cover the cycles TRAN, NEDC and SDMP detailed in Appendix D. The sample time for acquisition and bypassing is 20 ms. Furthermore, step tests are used for calibrating sensors and cycles for validating the model in dynamic state. If results are not satisfactory, dynamic cycles can be repeated and identifications checked. If the error persists, it could be advisable to come back to the static calibration and re-tune the incorrect parameters.

In the next, the results are presented.

6.2. Steady-state results

Top plots of Figure 13 show $x_{\mathrm{NO_x}}$ and $z_{\mathrm{NO_x}}$ for both ppm and g/h units as well as histogram plots of relative and absolute errors. The mean absolute error is 9.31 g/h with a mean relative error about 7%, and the standard deviation is σ=14.74 g/h, with a relative deviation of 9%. The model exhibits a better performance at high $\mathrm{NO_x}$ values, with maximum errors of 10%, while at low $\mathrm{NO_x}$ values, the maximum errors are about 30 %. For example, [33] present a $\mathrm{NO_x}$ model with maximum relative errors about 40% at high $\mathrm{NO_x}$ and 20% at low $\mathrm{NO_x}$ values. These results are in the line or indeed get better results than other approaches [46].

The results by evaluating ppm output present a mean error of 30.43 ppm and σ = 54.84 ppm, with relative mean error about 12% and a relative deviation of 11% respectively. As expected, the results are worse for the ppm output, but this is logical since the model has been calibrated for the ppm output. Alternatively, the part 2 of this paper introduces updating algorithms for the online correction of the model.

It is worth noting that errors of 1% in input variables can produce final $\mathrm{NO_x}$ errors of 33%, measured in a predictive and physics-based $\mathrm{NO_x}$ model, according tp the $\mathrm{NO_x}$ sensitivity study published in [38]. The maximum error in a data driven model, such as the one presented here, is bounded by the tables grid and only ageing and dispersion errors occurs, problems that exist also in more complex models. This fact and the results presented in this subsection justify the validity of a data-driven $\mathrm{NO_x}$ model, as well as the efficient computation and simple programming.

Medium and bottom plots of Figure 13 show absolute and relative error metrics for both outputs in g/h and ppm. Again, only a minimum percentage of points (total are 363) are out of the $\pm\sigma$ boundary, also plotted in those plots. If a higher accuracy on ppm output is required, tuning objective can be easily shifted to ppm.

Additional information from the model can be extracted to compare intermediate variables (calculated by model) and the corresponding measurements, as for instance for the mean value EGR flow model. A multi-objective optimisation could be programmed if other model states should be important for control. However, here $x_{\mathrm{NO_x}}$ output error has been minimised. Left plot of Figure 14 compares *EGR* calculated by the model and by using $[\mathrm{CO_2}]_{int}$ averaged from the 4 extractions of the in-cylinder manifolds. The fitting is acceptable in the whole range. Results for T_{egr} are shown in right plot of Figure 14, and the fitting in general is also acceptable, but there exists a high dispersion around the centre line. This is mainly due to areas with low or null EGR, where T_{egr} does not make any sense ($\dot{m}_{egr}$=0).

Model robustness. This section turns out the attention to the model robustness analysing the model sensitivity to errors in the main parameters and inputs. 2% disturbances in the parameters presented in Table 4 are applied and final variation in $\mathrm{NO_x}$ model output is stored, e.g. a change of 2% in n produce an error of 4.51% in $\mathrm{NO_x}$. Parameters with more influence on model output are n, m_f and $\dot{m}_a$. These signals basically represent the engine operating conditions, and define

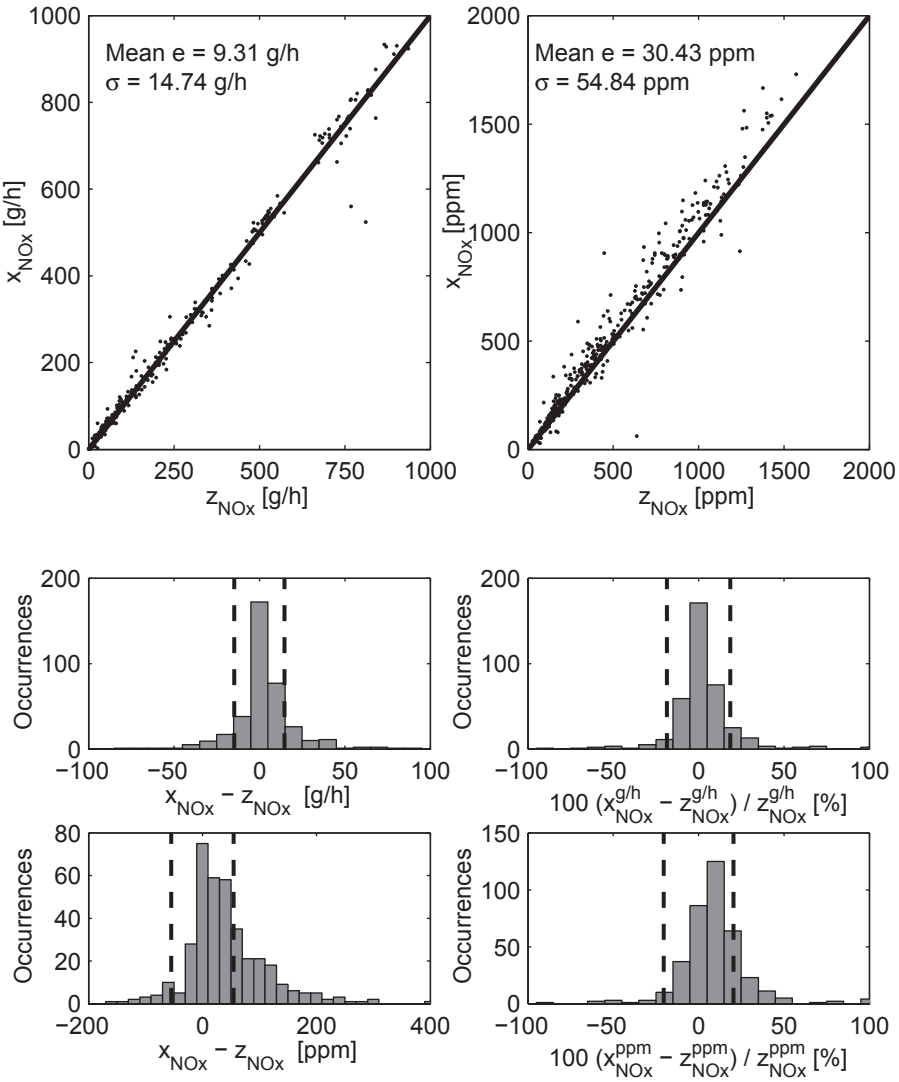

Figure 13: RT NO_x model results with steady tests. Top plots: Model fitting with respect to NO_x sensor output. Medium plots: Absolute and relative error in percentage with respect to NO_x sensor output and for g/h output ($x^{g/h}_{NO_x}$) of the model. Bottom plots: Absolute and relative error in percentage with respect to NO_x sensor output and for ppm output ($x^{ppm}_{NO_x}$) of the model.

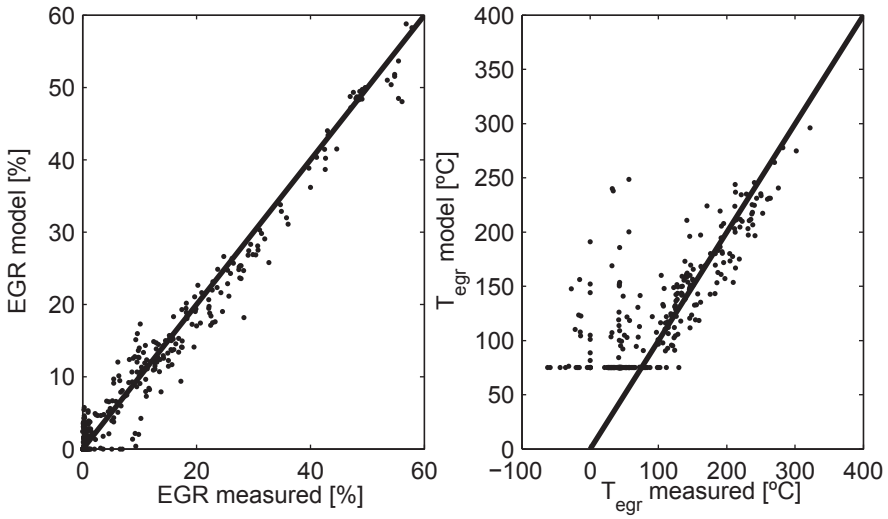

Figure 14: Relevant results from the EGR flow model. Left plot: calculated EGR from measurements.

the EGR setting (jointly with p_{boost} that presents a minor influence) and the trend was already expected. p_{boost} and η_v have the same influence as expected because both are multiplied for calculating $\dot{m}_{int}$ and consequently $\dot{m}_{egr}$.

An important conclusion of this study is that variables with more influence on NO_x are directly measured, and then having a reliable measurement is crucial for the model accuracy. In the second group, $NO_{x,0}$, $\dot{m}_{int}$ and η_v steady maps denote the most relevant maps to calibrate. The rest of variables have lower influence but not negligible.

Variable	Variation [%]	Mean error [%]	STD error [%]	Max. error [g/h]	Min. error [g/h]
n	+2	4.51	3.27	15.23	-1.41
m_f	+2	3.67	2.53	13.42	-0.36
m_{boost}	+2	3.42	3.50	12.60	-1.12
$NO_{x,0}$ MAP	+2	2	0.00	2.00	2.00
$\dot{m}_{int}$ MAP	-2	1.79	0.74	3.16	0.06
η_v MAP	-2	1.03	2.78	8.29	-2.93
p_{boost}	-2	1.03	2.78	8.29	-2.93
T_{cool}	+2	0.97	0.39	1.81	0.08
$EGR_0\lambda_0^{-1}$	+2	0.66	0.79	3.22	0.00
k_{egr} MAP	-2	0.16	0.31	1.39	-0.51
ΔT_{ie} MAP	+2	0.06	0.14	0.97	-0.14
k_{NO_x} MAP	+2	0.04	0.48	2.46	-2.42

Table 4: Result of applying variations of 2% to input variables over the final NO_x model output.

6.3. Dynamic results

Figure 9 already showed the ability of the NO_x model to fit the sensor and the necessity of utilising the factor C_{dyn}. Figure 15 shows the model results with the SDMP test. This test is a good benchmark for testing the dynamic ability of the model as fast transients are performed. The influence of C_{dyn} is remarkable and can be seen in the left plot of the figure. The absolute mean error for the SDMP cycles when using C_{dyn} is about 50 ppm against 75 ppm when using $C_{dyn} = 1$, which shows that an improvement in the estimation of 33 % is achieved. The standard deviation in ppm when using the factor C_{dyn} is in the order of 75 ppm, against 67 ppm when using $C_{dyn} = 1$.

In the SDMP, the influence of C_{dyn} is critical since the engine is ranging from low to high loads (thermal transients are critical). Right plot compares $y_{\mathrm{NO_x}}$ with NO_x sensor output with a good agreement indeed using ppm as output. Finally, the errors might be minimised when using online observers, as shown in part 2 of the paper.

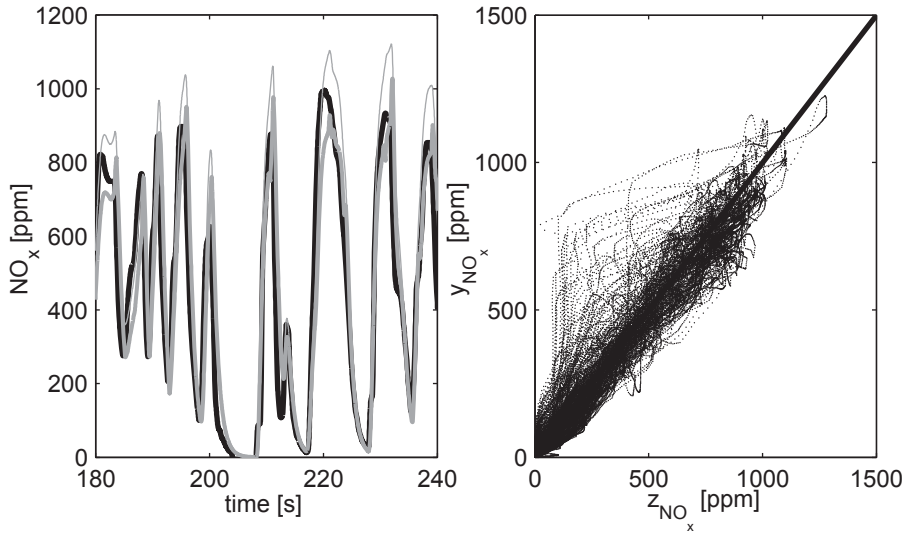

Figure 15: Left plot: $y_{\mathrm{NO_x}}$ calculated normally (thick gray) and cancelling thermal dynamic factor; i.e. $C_{dyn} = 1$ (thin gray), and NO_x sensor output $z_{\mathrm{NO_x}}$ (black) during a part of the SDMP B5. Right plot: $y_{\mathrm{NO_x}}$ against NO_x sensor output $z_{\mathrm{NO_x}}$.

Figure 16 shows results on the TRAN A ($T_{cool} = 75°C$, $\Delta u_{\mathrm{egr}} = 5\%$, $\Delta p_{boost} = 0$) cycle, left plot compares $y_{\mathrm{NO_x}}$ with $z_{\mathrm{NO_x}}$ while right plot includes also the $x_{\mathrm{NO_x}}$ estimation. The sensor model fits well enough to have a reliable $x_{\mathrm{NO_x}}$, that is observed by cancelling sensor filtering and lag. Even though the NO_x model is based on quasi-static maps, system and physics dynamics are contained in the model inputs, which are directly measured from sensors. As shown in the Figure, the results are also promising.

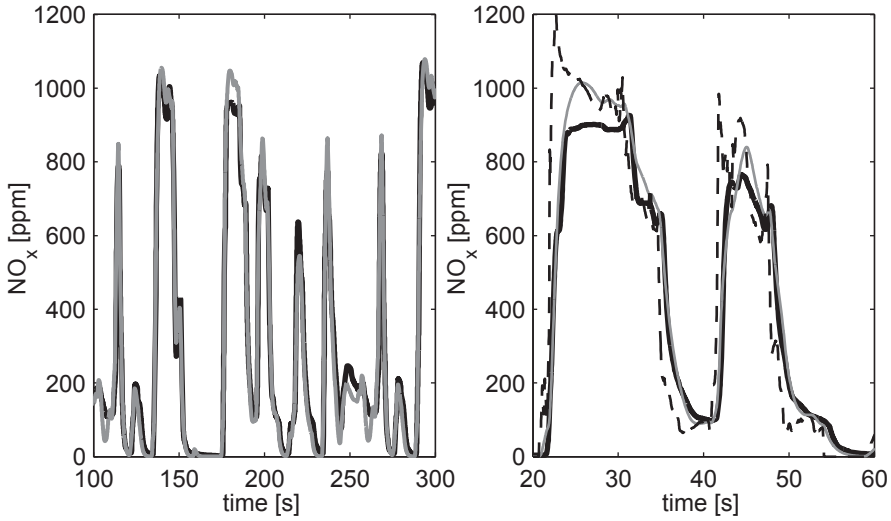

Figure 16: Left: $y_{\mathrm{NO_x}}$ (gray) and $z_{\mathrm{NO_x}}$ (black) in the TRAN A($T_{cool} = 75°C, \Delta u_{\mathrm{egr}} = 5\%, \Delta p_{boost} = 0$). Right: $x_{\mathrm{NO_x}}$ (dashed black), $y_{\mathrm{NO_x}}$ (thin gray) and $z_{\mathrm{NO_x}}$ (black) in the same test for a zoom. $x_{\mathrm{NO_x}}$ is the actual $\mathrm{NO_x}$ estimation, no delay nor filtering is expected.

The absolute mean value for $z_{\mathrm{NO_x}}$ and $y_{\mathrm{NO_x}}$ is calculated for every TRAN cycle

$$mean(y_{\mathrm{NO_x}}) = \frac{1}{l_{tran}} \sum_{k=1}^{l_{tran}} (abs(y_{\mathrm{NO_x}}(k))) \tag{40a}$$

$$mean(z_{\mathrm{NO_x}}) = \frac{1}{l_{tran}} \sum_{k=1}^{l_{tran}} (abs(z_{\mathrm{NO_x}}(k))) \tag{40b}$$

where l_{tran} is the total number of samples for every TRAN cycle. Results are plotted in Figure 17, where the left plot shows $mean(y_{\mathrm{NO_x}})$ against $mean(z_{\mathrm{NO_x}})$ while the right plot shows the error distributions in ppm. The results are quite good and the agreement is even better than for the SDMP, demonstrating the model accuracy.

The Figure 18 shows the results in the NEDC, by running the engine in warm conditions. $y_{\mathrm{NO_x}}$ prediction is better during the first 800 s of the cycle (the urban part). However, during the highway part, there exists a clear bias. Since the model is optimised for a set of steady-state tests, dispersion effects or errors due to non-modelled variables ($\mathrm{NO_x}$ is highly affected by the ambient conditions) can affect the model accuracy. Admittedly, the model dynamics are able to reproduce $z_{\mathrm{NO_x}}$ and then drift can be corrected by using observers.

7. Conclusions

An ECU oriented $\mathrm{NO_x}$ model has been developed by considering that variations of $[\mathrm{O_2}]_{int}$ cause exponential changes in nominal $\mathrm{NO_x}$, which is conveniently mapped. A study on different

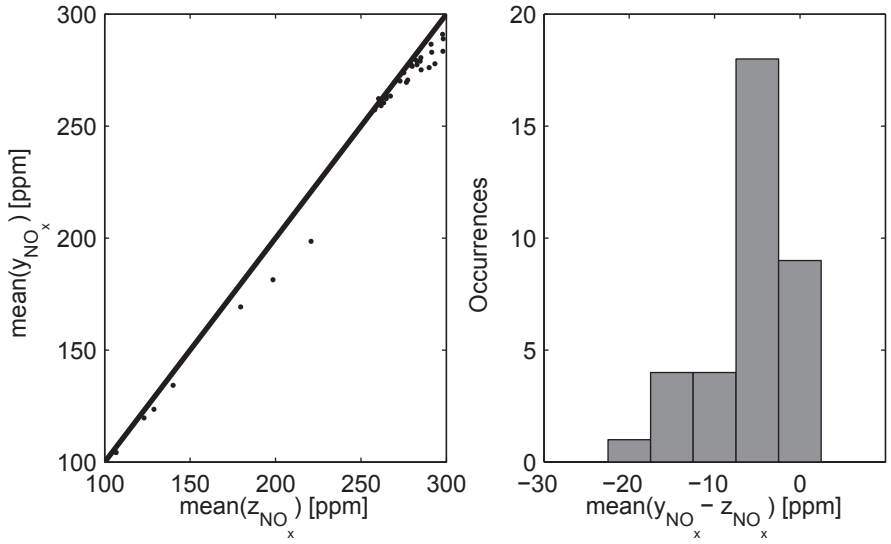

Figure 17: Left: Mean value of NO_x for sensor z_{NO_x} against model y_{NO_x} by simulating the NO_x model in all the TRAN cycles. Right: Absolute error $y_{NO_x} - z_{NO_x}$ bar distribution of the model against the sensor. The mean absolute error is less than 10%.

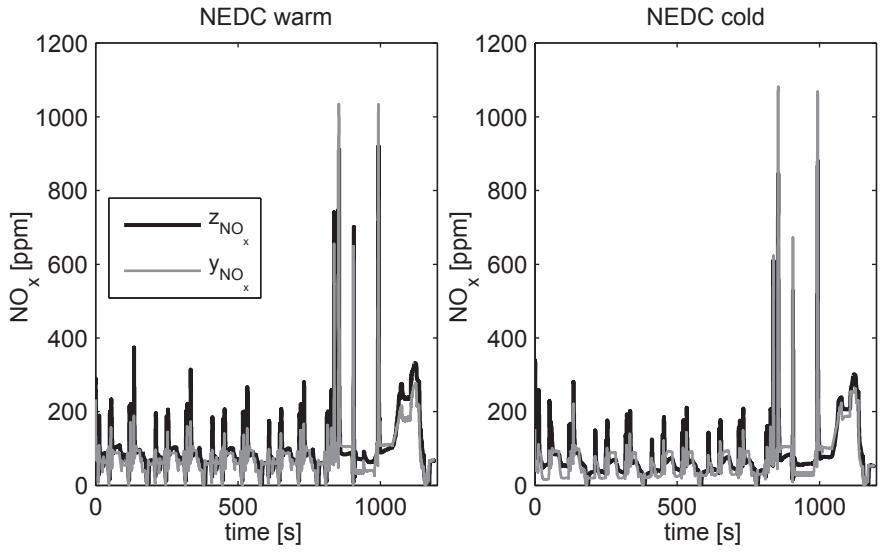

Figure 18: y_{NO_x} model output and z_{NO_x} measured by the sensor in the NEDC.

alternatives for estimating $[O_2]_{int}$ is presented in the paper, selecting the inert gas rate *EGR*. A set of corrections and factors with respect to nominal operating points are included for considering the most sensitive parameters. Furthermore, a thermal dynamic model for simulating cylinder temperature T_{cyl} is proposed as function of the product $\lambda^{-1}\ n$, which indirectly defines the engine thermal state. Two additional models are needed for the NO_x model: an EGR gray box model for estimating *EGR* and a Kalman filter for estimating fuel-to-air ratio λ^{-1} based on λ^{-1} signal from the NO_x sensor (alternatives are given if the sensor is not available).

A total of 363 steady-state tests are performed for calibrating all parameters and maps. Step-like tests for system and sensors identifications are made and TRAN, NEDC and a SDMP test are made in order to validate the model. The NO_x prediction is successful and the simple programming as well as the fact that all required signals are available in commercial ECUs makes the model suitable for online engine control or diagnosis.

[1] Bosch R. Automotive Handbook. 8th ed. Bosch Handbooks. Robert Bosch GmbH; 2011.

[2] EU. Regulation (EC) No 443/2009 of the European Parliament and of the Council of 23 April 2009 setting emission performance standards for new passenger cars as part of the Community's integrated approach to reduce CO_2 emissions from light-duty vehicles. Official Journal of the European Union; 2009.

[3] Heywood J. Internal Combustion Engine Fundamentals. McGraw Hill, New York; 1988.

[4] Arrègle J, López J, Guardiola C, Monin C. On Board NO_x Prediction in Diesel Engines: A Physical Approach. Automotive Model Predictive Control: Models, Methods and Applications, del Re L et al (Eds) ISBN-1849960704, Springer. 2010;.

[5] Zeldovich J. The Oxidation of Nitrogen Combustion and Explosions. Acta Physicochim. 1946;21(4):577–628.

[6] Lavoie G, Heywood J, Keck J. Experimental and Theoretical Study of Nitric Oxide Formation in Internal Combustion Engines. Combustion Science and Technology. 1970;1(4):313–326.

[7] Andersson M. Fast NO_x Prediction in Diesel Engines. Lund University; 2006.

[8] Desantes J, López J, Redón P, Arrègle J. Evaluation of the Thermal NO Formation Mechanism under Low-Temperature Diesel Combustion Conditions. International Journal of Engine Research. 2012;13(6):531–539.

[9] Brand D. Control-Oriented Modeling of NO Emissions of SI Engines. ETH Zürich; 2005.

[10] Luján J, Pla B, Moroz S, Bourgoin G. Effect of Low Pressure EGR on Gas Exchange Processes and Turbocharging of a HSDI Engine. THIESEL 2008 Conference on Thermo- and Fluid Dynamic Processes in Diesel Engines. 2008;.

[11] Timoney D, Desantes J, Hernndez L, Lyons C. The Development of a Semi-empirical Model for Rapid NO_x Concentration Evaluation Using Measured in-Cylinder Pressure in Diesel Engines. Proceedings of the Institution of Mechanical Engineers, Part D: Journal of Automobile Engineering. 2005;219(5):621–631.

[12] Guardiola C, Pla B, Blanco-Rodriguez D, Bares P. Cycle by Cycle Trapped Mass Estimation for Diagnosis and Control. SAE Int J Engines 7(3):2014. 2014;.

[13] Fleming W. Overview of Automotive Sensors. IEEE Sensors Journal. 2001;1(4):296–308.

[14] Payri F, Margot X, Gil A, Martín J. Computational Study of Heat Transfer to the Walls of a DI Diesel Engine. SAE Technical Paper 2005-01-0210. 2005;.

[15] Woschni G. A Universally Applicable Equation for the Instantaneous Heat Transfer Coefficient in the Internal Combustion Engine. SAE Technical Paper 670931. 1967;.

[16] Arrègle J, López J, Martín J, Mocholí E. Development of a Mixing and Combustion Zero-Dimensional Model for Diesel Engines. SAE Technical Paper 2006-01-1382. 2006;.

[17] Payri F, Olmeda P, Martín J, García A. A Complete 0D Thermodynamic Predictive Model for Direct Injection Diesel Engines. Applied Energy. 2011;88(88):4632–4641.

[18] Guardiola C, López J, Martín J, García-Sarmiento D. Semiempirical in-Cylinder Pressure based Model for NO_x Prediction Oriented to Control Applications. Applied Thermal Engineering. 2011;31(16):3275–3286.

[19] Westlund A, Winkler N, Diotallevi F, Ångström H. Predictions and Measurements of Transient NO Emissions for a Two-stage Turbocharged HD Diesel Engine with EGR. In: Thiesel 2008 Conference on Thermo-Fluid Dynamics Processes in Diesel Engines. Valencia, Spain; 2008. .

[20] Andersson I, Eriksson L. A Parametric Model for Ionization Current in a Four Stroke SI Engine. ASME. 2009;.

[21] Eriksson L, Andersson I. An Analytic Model for Cylinder Pressure in a Four Stroke SI Engine. SAE Technical Paper 2002-01-0371. 2002;Available from: http://papers.sae.org/2002-01-0371/.

[22] Westlund A. Simplified Models for Emission Formation in Diesel Engines during Transient Operation. KTH Industrial Engineering and Management; 2011.

[23] Arsie I, Pianese C, Rizzo G. An Integrated System of Models for Performance and Emissions in SI Engines: Development and Identification. SAE Technical Paper 2003-01-1052. 2003;.

[24] Karlsson M, Ekholm K, Strandh P, Tunestål P, Johansson R. Dynamic Mapping of Diesel Engine through System Identification. In: Proc. American Control Conference. Baltimore, MD; 2010. .
[25] Hirsch M, Alberer D, del Re L. Grey-Box Control Oriented Emissions Models. In: Proceedings of the 17th World Congress, The International Federation of Automatic Control, Seoul, Korea, July 6-11; 2008. .
[26] Takagi T, Sugeno M. Fuzzy Identification of Systems and Its Applications to Modeling and Control. IEEE Transactions on Systems, Man and Cibernetics. 1985;SMC-15, No 1, January/February.
[27] Lughofer E, Macián V, Guardiola C, Klement E. Identifying Static and Dynamic Prediction Models for NO_x Emissions with Evolving Fuzzy Systems. Applied Soft Computing. 2011;11:2487–2500.
[28] Falck T, Dreesen P, De Brabanter K, Pelckmans K, De Moor B, Suykens J. Least-Squares Support Vector Machines for the identification of Wiener-Hammerstein systems. Control Engineering Practice. 2012;20(11):1165–1174.
[29] Yen G, Michel A. A Learning and Forgetting Algorithm in Associative Memories: Results Involving Pseudo Inverses. In: IEEE International Symposium on Circuits and Systems; 1991. p. 778 –781 vol.2.
[30] Alonso J, Alvarruiz F, Desantes J, Hernández L, Hernández V, Moltó G. Combining Neural Networks and Genetic Algorithms to Predict and Reduce Diesel Engine Emissions. IEEE Transactions on Evolutionary Computation. 2007;11(1):46–55.
[31] Maa B, Stobart R, Deng J. Diesel Engine Emissions Prediction Using Parallel Neural Networks. Proceedings of the American Control Conference. 2009;p. 1122–1127.
[32] Arsie I, Pianese C, Sorrentino M. Development of Recurrent Neural Networks for Virtual Sensing of NO_x Emissions in Internal Combustion Engines. SAE International Journal of Fuels and Lubricants. 2010;2(2):354–361.
[33] Schilling A, Amstutz A, Onder C, Guzzella L. A Real-Time Model for the Prediction of the NO_x Emissions in DI Diesel Engines. In: Proceedings of the 2006 IEEE International Conference on Control Applications. Munich, Germany; 2006. .
[34] Desantes J, Luján J, Guardiola C, Blanco-Rodriguez D. Development of NO_x Fast Estimate Using NO_x Sensors. In: EAEC 2011 Congress. Valencia; 2011. .
[35] Luján J, Galindo J, Serrano J, Pla B. A Methodology to Identify the Intake Charge Cylinder-to-Cylinder Distribution in Turbocharged Direct Injection Diesel Engines. Measurement Science and Technology. 2008;19(6).
[36] Andersson M, Hultqvist A, Johansson B, Nöhre C. Fast Physical NO_x Prediction in Diesel Engines. In: The Diesel Engine: The Low CO2 and Emissions Reduction Challenge (Conference Proceedings), Lyon; 2006. .
[37] Galindo J, Serrano J, Guardiola C, Blanco-Rodriguez D, Cuadrado I. An on-engine method for dynamic characterisation of NO_x concentration sensors. Experimental Thermal and Fluid Science. 2011;35(3):470–476.
[38] Arrègle J, López J, Guardiola C, Monin C. Sensitivity Study of a NO_x Estimation Model for on-Board Applications. SAE Tecnhical Report 2008-01-0640. 2008;Available from: http://papers.sae.org/2008-01-0640/.
[39] Broatch A, Luján J, Serrano J, Pla B. A Procedure to Reduce Pollutant Gases from Diesel Combustion during European MVEG-A Cycle by Using Electrical Intake Air-Heaters. Fuel. 2008;87(12):2760–2778.
[40] Wahlström J, Eriksson L. Modelling Diesel Engines with a Variable-Geometry Turbocharger and Exhaust Gas Recirculation by Optimization of Model Parameters for Capturing Non-Linear System Dynamics. Proceedings of the Institution of Mechanical Engineers, Part D: Journal of Automobile Engineering. 2011;225(7):960–986.
[41] Arsie I, Di Leo R, Pianese C, De Cesare M. Combustion Noise and Pollutants Prediction for Injection Pattern and EGR Tuning in an Automotive Common-Rail Diesel Engine. ECOSM 2012 Workshop on Engine and Powertrain Control, Simulation and Modeling. 2012;.
[42] Galindo J, Climent H, Guardiola C, Doménech J. Strategies for Improving the Mode Transition in a Sequential Parallel Turbocharged Automotive Diesel Engine. International Journal of Automotive Technology. 2009;10(2):141–149.
[43] Guardiola C, Pla B, Blanco-Rodriguez D, Mazer A, Hayat O. A bias correction method for fast fuel-to-air ratio estimation in diesel engines. Proceedings of the Institution of Mechanical Engineers, Part D: Journal of Automobile Engineering. 2013;227(8):1099–1111.
[44] Galindo J, Luján J, Climent H, Guardiola C. Turbocharging System Design of a Sequentially Turbocharged Diesel Engine by Means of a Wave Action Model. SAE Technical Paper 2007-01-1564. 2007;.
[45] HORIBA. Horiba MEXA-7000DEGR Instruction Manual; 2001.
[46] Winkler-Ebner B, Hirsch M, del Re L, Klinger H, Mistelberger W. Comparison of Virtual and Physical NO_x-Sensors for Heavy Duty Diesel Engine Application. SAE International Journal of Engines. 2010;3(1):1124–1139.

Appendix A. Acronyms

CAN	Controller area network
CO	Carbon monoxide

CO_2	Carbon dioxide
DI	Direct injection
ECU	Electronic control unit
EGR	Exhaust gas recirculation
ETK	Ethernet based ECU conection
FTP	Federal test procedure
HW	Hammertein-Wiener
LD	Light duty
LNT	Lean NO_x trap
NEDC	New European driving cycle
NN	Neural network
NO	Nitrogen monoxide
NO_2	Nitrogen dioxide
NO_x	Nitrogen oxides (NO + NO_2)
O_2	Oxygen
OBD	On-board diagnostics
OEM	Original equipment manufacturer
PM	Particulate matter
RT	Real time
SCR	Selective catalyst reduction
SI	Spark ignition
SKF	Simplified Kalman filter
SOI	Start of injection
UEGO	Universal exhaust gas oxygen
WG	Waste-gate

Table A.5: Relevant acronyms used in the paper.

Appendix B. Variables and abbreviations

u_{wg}	Waste-gate valve position command 0-open, 100-closed	%
u_{egr}	EGR valve position command 0-open, 100-closed	%
u_α	Pedal position command	%
u_{vgt}	VGT position command	%
$\dot{m}$	Mass flows	kg/h
m	Mass per stroke	mg/str
p	Pressures	bar
T	Temperatures	K (°C)
$\dot{m}_a$	Air mass flow	kg/h
$\dot{m}_a^*$	$\dot{m}_a$ set-point reference for controller	kg/h
$\dot{m}_f$	Injected fuel mass flow	kg/h

m_f	Injected fuel mass	mg/str
t_{mi}	Main injection duration	μs
p_{boost}	Boost pressure	bar
p^*_{boost}	p_{boost} set-point reference for controller	bar
T_{cool}	Engine coolant temperature	K (°C)
T_{exh}	Exhaust temperature	K (°C)
T_{int}	Intake temperature	bar
p_{exh}	Exhaust pressure	bar
p_{int}	Intake pressure	bar
T_{wic}	Temperature of the water of the intercooler	K (°C)
T_{egr}	EGR temperature	K (°C)
n	Engine speed	rpm
p_{rail}	Rail pressure	bar
I_p	Current output from the UEGO sensor	mA
η_v	Volummetric efficiency	-
EGR	EGR rate	%
H	Humidity	%
z	Sensor measurements	-
X	State-vector	-
U	Input vector	-
Y	Output vector	-
τ	Sensor delay	s (or ms)
a	Discrete response time parameter	-
T_s	Sample time	ms
t	time	s
k	Discrete instant	-
z	Z-transform variable	-
$a_{\mathrm{NO_x}}$	Discrete response time of the NO_x output	-
$\tau_{\mathrm{NO_x}}$	Delay of the NO_x output	μs
$z_{\mathrm{NO_x}}$	NO_x output from the NO_x sensor	ppm
$x_{\mathrm{NO_x}}$	Output from the NO_x model	g/h (or ppm)
$y_{\mathrm{NO_x}}$	Filtered and delayed output from the NO_x model	g/h (or ppm)
$x_{\mathrm{NO_x}f}$	Filtered and delayed output from the NO_x model in the state-space model	g/h (or ppm)
$z_{\lambda^{-1}}$	λ^{-1} output from the NO_x sensor	-
x_λ^{-1}	λ^{-1} model from the fuel-to-air ratio calculation	-
y_λ^{-1}	Filtered and delayed output from the λ^{-1} model	-
$x_{\lambda^{-1}f}$	Filtered and delayed output from the λ^{-1} model in the state-space model	-
$C_{\mathrm{NO_x}}$	Correction factor for NO_x model	-
C_{dyn}	Dynamic thermal loading factor for NO_x model	-
k	With subscript: Correction to the NO_x model	-

C	With subscript: Correction to the NO_x model	-

Table B.6: Relevant symbols and variables used in the paper.

Appendix C. Selection of the units for the NO_x model output

Sensor raw signal is measured in ppm, which indicates the relative molar concentration of NO_x, but the final NO_x mass depends on the exhaust mass flow and time. The conversion from ppm to g/h used in this work is

$$\dot{x}_{\mathrm{NO_x}}^{g/h} = 0.001587 x_{\mathrm{NO_x}}^{ppm} \cdot (\dot{m}_a^{kg/h} + \dot{m}_f^{kg/h}) \tag{C.1}$$

considering that molecular mass of NO_x is 46.1 g/mol and exhaust mass flow density is 1.293 kg/m^3, measured at 273 K and 101.3 KPa. The conversion of mg/str to kg/h for a 4 cylinder 4-strokes engine, provided that n is given in rpm, is as follows

$$\dot{m}^{kg/h} = 4 \cdot \frac{n}{2} \cdot \frac{60}{10^6} \cdot m^{mg/str} \tag{C.2}$$

The use of mass flow variables is appropriate for taking into account total emissions and calculating the real impact on the environment. In addition, after-treatment devices such as LNT require a count of cumulated NO_x for trap regeneration. Then, mass flow seems also suitable for OBD purposes.

For computing total NO_x emissions, $\dot{x}_{\mathrm{NO_x}}^{g/h}$ can be integrated in the considered cycle

$$M_{\mathrm{NO_x}}^{g} = \int_{t_1}^{t_2} \dot{x}_{\mathrm{NO_x}}^{g/h} dt \tag{C.3}$$

where M stands for total mass.

Commercial NO_x sensors measure the relative volume flow of NO_x in parts per million (ppm) and the conversion to g/h can induce some error, especially if $\dot{m}_a$ presents some drift or filtering effect. Anyway, the use of g/h for online NO_x tracking is justified for two reasons: (1) dilution effects are avoided as ppm is a relative measurement and (2) the use of g/h is coincident with the actual emissions. Dilution effects can distort the ppm output and can lead to sign shifts in the gradient when comparing ppm output and g/h at high load conditions (no EGR), i.e. an increase of g/h could result in a decrease of ppm if $\dot{m}_a$ increases. On the other hand, minimum variations of g/h can lead to huge variations in ppm even though the relative gradient could be high in both two, especially at low load conditions (related with low $\dot{m}_a$), leading to overestimate NO_x emissions when tracking ppm. In this work, the NO_x model output is calibrated for minimising the error on g/h, even though ppm output is also provided.

Appendix D. Engine cycles

The following cycles have been performed on the engine.

Adapted Transient cycles (TRAN). A set of dynamic tests are designed on the basis of two different modifications of the FTP cycle for HD engines (named here as TRAN A and TRAN B), and are used for training and evaluating the NO_x model in transient operation. These consist of a scaling of the central part of the standard FTP and are compared in Figure D.19. Test proposition is a full factorial design by performing modifications on set-points for u_{egr} (by modification on the $\dot{m}_a$ maps), p_{boost} (by fixing $\dot{m}_a$ set-point and modifying p_{boost} map) and T_{cool} (modifying the coolant reference temperature at the test cell controller). The sequence is presented in Table D.7, totalling 36 different tests (27 TRAN A and 9 TRAN B). For each test, three repetitions of the sequence shown in Figure D.19 are made.

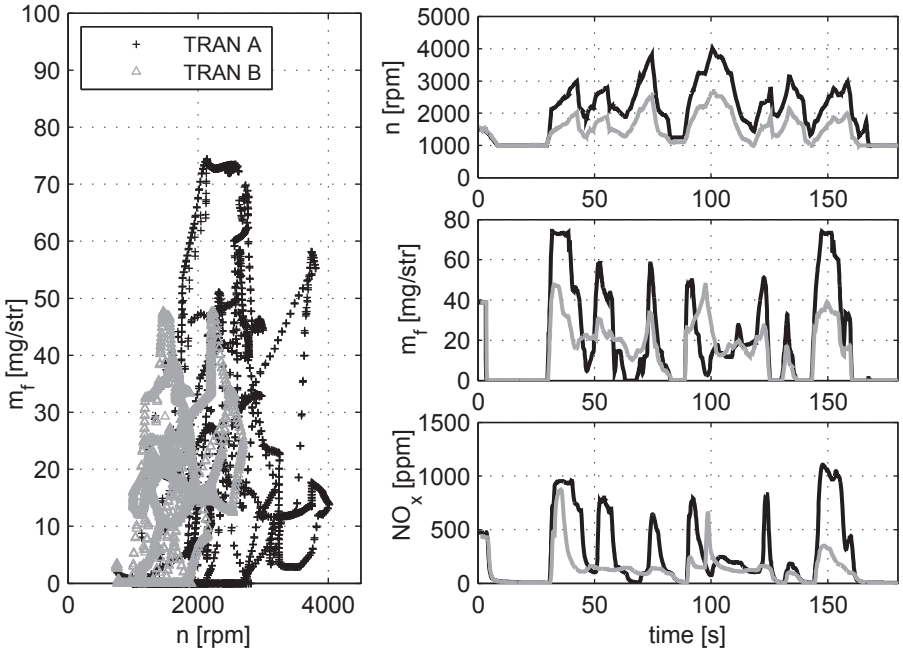

Figure D.19: TRAN nominal cycles designed for the model validation

NO_x sensitivity to variations on inputs and parameters is considerably lower for transient than static conditions. This fact is due to the systems and sensors dynamics which filter the effects. For instance, the effect of varying 10°C in T_{cool} and in the TRAN A cycle produces variations around 10% in NO_x. An increasing of 10% in p_{boost} (100 mbar) in the TRAN A cycle leads to an increase NO_x around 10%, while in steady conditions produces an increase in the order of 40% for the same conditions (while fixing $\dot{m}_a$ set-point in the EGR area of the engine). The EGR variations are made by $\dot{m}_a$ set-point modifications. In all cases, the higher NO_x sensitivity is found for EGR variations, especially for TRAN B cycles, which have sharper EGR transients. Figure D.20 shows the effect of modifying EGR rate (by plotting $[CO_2]_{int}$) over the final NO_x emissions measured by the sensor.

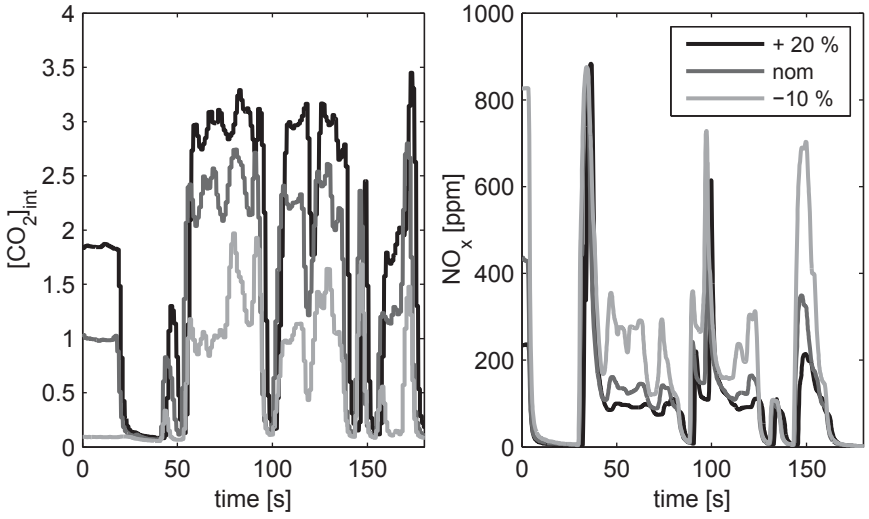

Figure D.20: $[CO_2]_{int}$ at intake and NO_x emissions for TRAN B varying EGR

cycle	T_{cool} [°C]	Δu_{egr}[%]	Δp_{boost} [mbar]
TRAN A	[75,85,95]	[-5,0,+5]	[-100,0,+100]
TRAN B	nom	[-10,0,+20]	[-100,0,+100]

Table D.7: Experimental plan of modified TRAN cycles

New European Driving Cycle (NEDC). The NEDC is tested in warm-start conditions (at the beginning of the test). The cycle consists of a urban part with accelerations/decelerations and idling, and an extra-urban part that lasts 400 s. The urban part has 4 equal repetitions of a sequence that lasts 200 s; Figure D.21 shows last repetition of the urban part and extra-urban section.

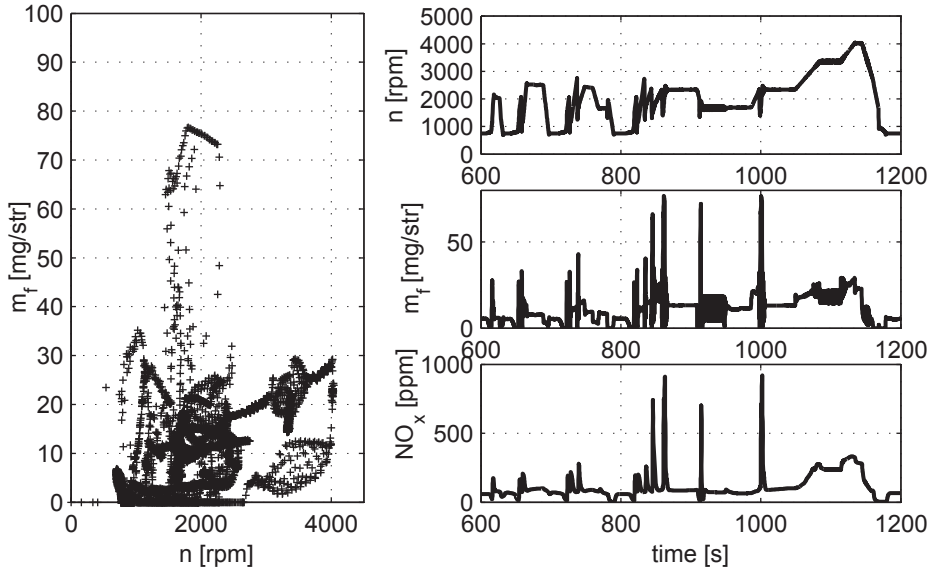

Figure D.21: NEDC cycle performed on the engine at warm conditions.

Common Artemis Driving Cycles (CADC). CADC are designed upon the basis of an statistical analysis of European real world driving patterns, developed by the European Artemis project (Assessment and Reliability of Transport Emission Models and Inventory Systems). The cycle includes three different variants: urban, rural road and highway. These profiles are more realistic than NEDC as they cover different real situations and then constitute a good source for experimental testing. The urban version has been tested for the paper and it is shown in Figure D.22.

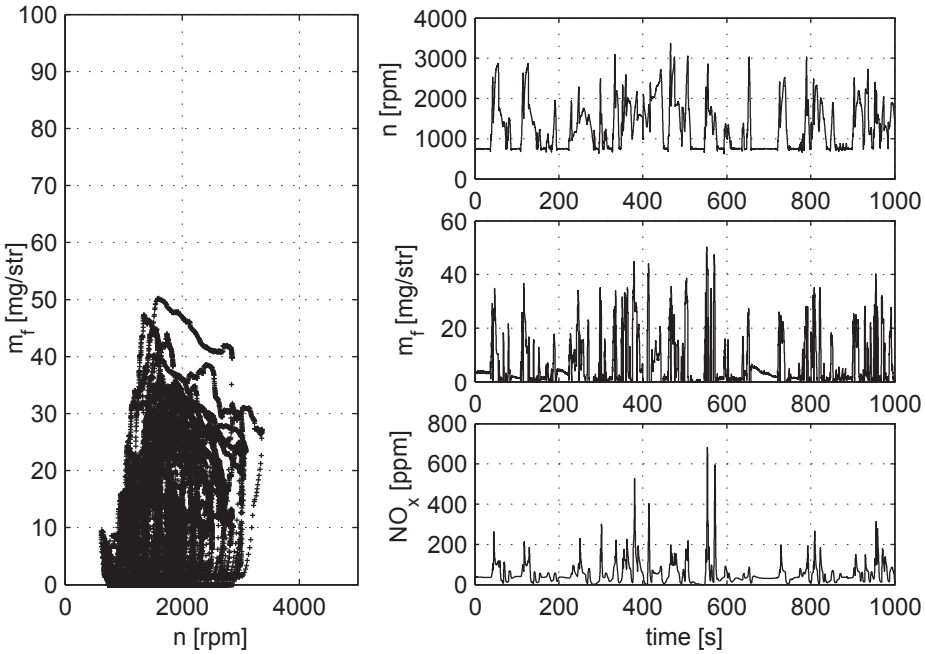

Figure D.22: Urban CADC cycle performed on the engine.

Sportive driving mountain profile (SDMP). The SDMP is designed for covering a wide operating range of the engine by sharp variations on n and m_f. A zoom on 400 seconds (total is 1200) of the SDMP is shown in Figure D.23 (Left plot indicates the whole cycle points). Since SDMP presents sharp load transients, the EGR valve is mostly closed during the cycle, making that $EGR = 0$ during the major part in spite of the engine might be run in the EGR area. This circumstance distorts the closed loop nominal engine operation.

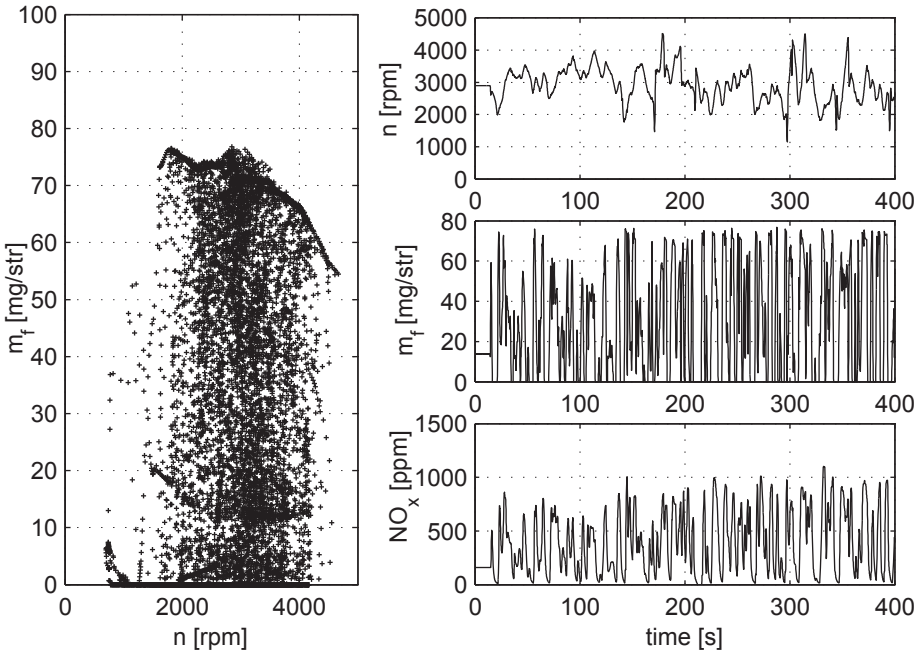

Figure D.23: SDMP cycle performed on the engine.